Article

Not peer-reviewed version

Toxicological study of kaempferol and linearolactone as treatments for amoebic liver abscess development in Mesocricetus auratus.

Luis Varela-Rodríguez , Fernando Calzada , José Antonio Velázquez-Domínguez , Verónica Ivonne Hernández-Ramírez , Hugo Varela-Rodríguez , Elihú Bautista , Mayra Herrera-Martínez , Rodrigo Daniel Castellanos-Mijangos , Bibiana Chávez-Munguía , Patricia Talamás-Rohana *

Posted Date: 10 July 2024

doi: 10.20944/preprints202407.0797.v1

Keywords: Absceso hepático amebiano; Entamoeba histolytica; Kaempferol; Linearolactona; Mesocricetus auratus; Toxicidad.

Article

Toxicological Study of Kaempferol and Linearolactone as Treatments for Amoebic Liver Abscess Development in *Mesocricetus auratus*

Luis Varela-Rodríguez [1,†], Fernando Calzada [2], José Antonio Velázquez-Domínguez [3,†], Verónica Ivonne Hernández-Ramírez [3], Hugo Varela-Rodríguez [1,4], Elihú Bautista [5], Mayra Herrera-Martínez [6], Rodrigo Daniel Castellanos-Mijangos [7], Bibiana Chávez-Munguía [3] and Patricia Talamás-Rohana [3,*]

[1] Facultad de Ciencias Químicas, UACH; CP 31125, Chihuahua, CHIH, México; vrodriguez@uach.mx
[2] Unidad de Investigación Médica en Farmacología, Hospital de Especialidades UMAE-CMNSXXI-IMSS; CP 06725, CDMX, México; fercalber10@gmail.com
[3] Departamento de Infectómica y Patogénesis Molecular, CINVESTAV-IPN; CP 07360, CDMX, México; jauam14@yahoo.com.mx (J.A.V.D.); arturomvi@hotmail.com (V.I.H.R.); bchavez@cinvestav.mx (B.C.M.)
[4] Facultad de Medicina y Ciencias Biomédicas, UACH; CP 31109, Chihuahua, CHIH, México; hvrodriguez@uach.mx
[5] Unidad de Ciencias Ambientales, IPICYT; CP 78216, San Luis Potosí, SLP, México; hormigaqfb@hotmail.com
[6] Instituto de Farmacobiología, UNCA; CP 68540, Teotitlán de Flores Magón, OAX, México; chimay_2002@hotmail.com
[7] Unidad de Imagenología Diagnóstica, ISSEMyM-Arturo Montiel Rojas; CP 52170, Metepec, MEX, México; rodan_casmij@hotmail.com
* Correspondence: ptr@cinvestav.mx; Tel.: [01+52]-(55)-5747-3351
† First authors: L.V.R. and J.A.V.D. contributed equally to this work and share authorship.

Abstract: Several studies with kaempferol (KP) and linearolactone (LL) have shown antiparasitic activities. However, the toxicity of treatments with both active principles is unknown. Therefore, this study aimed to evaluate the toxicological effects of treatments with KP and LL on the amoebic liver abscess (ALA) model in *M. auratus* administered intraperitoneally (i.p.). For this, ALA induction was carried out in male hamsters with 1.5 x10^5 *E. histolytica* trophozoites inoculated in the left hepatic lobe. The lesion evolved for four days and the i.p. of the treatments with KP (5 mg/kg body weight/day) and LL (10 mg/kg body weight/day) was carried out for four consecutive days. For histopathological evaluation, NMR studies, paraclinical analysis, and necropsy were performed. The results revealed that the inhibition of ALA by KP and LL were similar to that metronidazole (MTZ). Biochemical parameters revealed hepatic and renal alterations in all treatment groups, mainly for KP (AST and BUN). The lesions found in the organs were those that are directly linked to the pathology. In conclusion, KP and LL decrease ALA development but have few toxicological effects. Both compounds combined with MTZ could be therapeutic alternatives for amoebiasis caused by *E. histolytica*.

Keywords: amoebic liver abscess; *Entamoeba histolytica*; kaempferol; linearolactone; *Mesocricetus auratus*; toxicity

1. Introduction

Worldwide, diarrheal diseases are important for public health due to the high rates of morbidity and mortality in children [1,2]. Despite being preventable and treatable diseases, they are the second

 doi:10.20944/preprints202407.0797.v1

cause of death in children under five years of age [1]. Among the etiological agents that cause diarrhea are bacteria, viruses and protozoa, such as *Escherichia coli (E. coli)*, *Rotavirus*, *Giardia lamblia* (*G. lamblia*) and *Entamoeba histolytica* (*E. histolytica*) [1]; This latter pathogen causes acute diarrhea, dysentery, fulminant colitis, amoeboma, and liver abscesses [2].

There is a high incidence of childhood amoebiasis, caused by *E. histolytica* in third world countries [1]. The infection is acquired after ingestion of food or water contaminated with cysts, while colonization occurs in the intestine, breakdown of the defense system and lysis of epithelial cells by trophozoites [2]. Clinically, the most common treatment is metronidazole (MTZ); However, various studies (*in vitro* and *in vivo*) have emphasized the development of resistance mechanism [3,4]; in addition, MTZ has been related to several medical complications, such as hypersensitivity, neutropenia, peripheral neuropathies, and cancer [5–7]. This has contributed to the search for new molecules that carry out antiparasitic treatments that do not compromise the morphophysiological integrity of the individual's body compartments [8].

In this sense, traditional medicine represents a great opportunity to search for the effect of new therapeutic agents. Previous studies have shown the antiprotozoal activity of two active principles kaempferol (KP), a flavonoid, and linearolactone (LL), a diterpene, obtained from the aerial parts of the plants *Cuphea pinetorum* Benth. (*C. pinetorum*) and *Salvia polystachya* Ort. (*S. polystachya*), known in Mexico as "*Bakmomol*" and "*chia*" respectively. The effectiveness of KP has been evidenced in trophozoites of *E. histolytica* (IC_{50}: 27.7 μM) and *G. lamblia* (IC_{50}: 30.4 μM) [8–10]. Its main effects alter cellular functions by decreasing adhesion and increasing migration and phagocytic activity due to overexpression of cytoskeletal proteins such as actin, myosin-II and cortexillin-II [9,11]. For its part, LL has exhibited greater antiproliferative activity in the trophozoites of *E. histolytica* (IC_{50}: 22.9 μM) and *G. lamblia* (IC_{50}: 28.2 μM), since it induces cellular alterations, such as chromatin condensation, intracellular ROS production, and loss of cellular structures. This compound showed cell death by apoptosis in *E. histolytica* while in *G. lamblia* it showed an effect of death by necrosis [10–14].

Despite the excellent antiprotozoal activity exhibited by KP and LL, to date there are no studies demonstrating their possible toxicological effects during the treatment of amoebiasis. Toxicological evaluation of antiamoebic therapies is relevant because *E. histolytica* crosses the intestinal epithelium and migrates to the liver to induce the development of amoebic liver abscess (ALA). ALA is a common complication of amoebiasis and is characterized by a purulent infiltrate in various areas of the liver. Furthermore, ALA also limits a number of vital liver functions, such as metabolism, immunity, digestion, detoxification, and vitamin storage [2,15]. Therefore, severe liver dysfunction in patients with ALA can lead to various medical complications, such as hepatic encephalopathy, jaundice, toxicity, infections, multiple organ failure, and ultimately death [16]. Therefore, the present work focuses its attention on evaluating the possible toxicological effects of the intraperitoneal administration of KP and LL against ALA in *Mesocricetus auratus* (*M. auratus*).

2. Results and Discussion

2.1. Cytotoxic Effect of the Active Principles Kp and LL in Cell Lines

Our objective was to analyze the effects that the flavonoid KP and the diterpene LL induced directly on E. histolytica, CHO-K1 or BEAS-2B. To this end, by flow cytometry it was observed that treatments with KP and LL reduce 50% cell viability in virulent HM1 trophozoites at 31.6 and 7.8 μg/mL respectively, compared to MTZ (positive control), of 0.16 μg/mL or 1X PBS (negative control) for 48 h ($p \leq 0.05$, Dunnett) (Table 1). These results demonstrated that E. histolytica is more sensitive to the effect of LL, compared to KP, possibly due to the nature of the active principles evaluated (Figure S1). On the other hand, on normal cells it was observed that KP had the most significant inhibitory effect on CHO-K1 and BEAS-2B cells (IC_{50}: 70/100 μg/mL), compared to treatments with LL (IC_{50}: 300/200 μg/mL), or vehicle (Vh) after 24 h ($p \leq 0.05$, Dunnett) (Figure 1). These data suggest that the effect of both active principles is possibly due to the characteristic phenotype of the cells. However, both active substances showed the strongest inhibition (Figure 1) and therefore a low selectivity index compared to MTZ, possibly due to differences in their mechanism of action. Finally,

 doi:10.20944/preprints202407.0797.v1

KP and LL showed a theoretical LD_{50} of 552 and 824 mg/kg body weight respectively for the oral route, while MTZ presented a dose of 1,026 mg/kg body weight (Table 1), these results suggest that KP might be more toxic compared to LL.

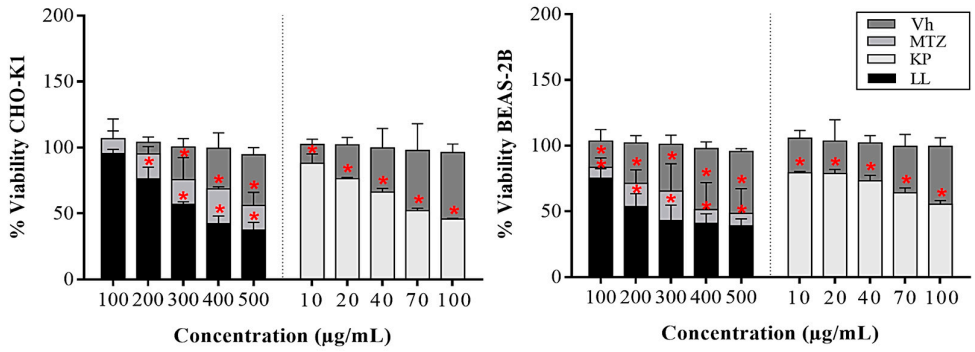

Figure 1. Cytotoxic effect of the active principles KP and LL on the CHOK-1 and BEAS2B cell line. The half-maximal inhibitory concentrations (IC_{50}) of KP and LL in CHO-K1 and BEAS-2B cell lines were determined by dose-response viability curves after 24 h using the MTT assay. Results show the mean ± SD of three biological replicates (n = 3, in triplicates). (*) $p \leq 0.05$ vs. vehicle (1X PBS, negative control), ANOVA. Metronidazole was used as positive control (antiparasitic reference).

Table 1. Toxicological activities of KP and LL in cell lines.

***In vitro* studies: IC_{50}, SI and LD_{50}**				
Samples	**Vh**	**MTZ**	**KP**	**LL**
IC_{50} HM-1	Innocuous	0.16 ++ *	31.6 + *	< 7.8 + *
IC_{50} CHO-K1	Innocuous	500 - *	70 +/- *	300 - *
IC_{50} BEAS-2B	Innocuous	400 - *	100 +/- *	200 - *
SI	ND	3,461 ++	2.7 +/-	> 32 +
LD_{50} (Theoretical)	ND	1,025.64	551.75	824.20

Symbols correspond to the biological activity of the samples: ++, very high; +, high; +/-, medium; -, low; and --, very low. The selectivity index (SI) indicates specific activity on normal cells vs. trophozoites (µg/mL). LD_{50}, median lethal dose (oral, mg/kg). ND, not determined. Results show the mean ± SD of three biological replicates (n = 3, in triplicates). (*) $p \leq 0.05$ vs. vehicle (1X PBS, negative control), ANOVA. Metronidazole was used as positive control (antiparasitic reference).

2.2. Treatment with KP or LL Selectively Induced Cell Death and Morphological Alterations in Trophozoites versus Normal Cells

By flow cytometry it was observed that individual treatments on *E. histolytica* trophozoites with MTZ (0.16 µg/mL), KP (31.6 µg/mL), and LL (15.6 µg/mL), induced a decrease in size and granularity in the cell population of 52, 55, and 66% respectively (Figure S1A), compared with the Vh group after 48 h in a dose-dependent manner ($p \leq 0.05$, Dunnett). Furthermore, under the same treatment conditions, trophozoites showed apoptotic and necrotic events when treated with KP (8.2/45.2%) and LL (4.3/90.1%) in a dose-dependent manner (Figure S1B). These effects were similar with MTZ (2/62.2%) compared to the Vh group in both cases ($p \leq 0.05$, Dunnett). In this sense, high doses of LL appear to be necrotic inductor much more potent compared to KP, particularly. A clear evidence of apoptosis induction is the externalization of phosphatidylserine and alterations in the permeability of the cell membrane. These findings were corroborated by TEM and correlated with results obtained by confocal microscopy (Figure S1C, upper panel), through which we observe the binding of annexin-V to phosphatidylserine in all cells treated with the active principles. The necrotic events observed during treatments with both active principles may be related to the late stage of apoptosis and not to true necrosis, which can promote inflammatory processes; However, additional studies are needed

 doi:10.20944/preprints202407.0797.v1

to corroborate these findings. Additionally, confocal microscopy revealed that KP and LL treatments induced arrest of mitotic cell division (binary fission type) and alterations in the actin cytoskeleton showing atypical cells (Figure S1). In particular, cells treated with KP present disorganization of the actin microfilaments, while cells treated with LL present little polymerizate actin (Figure S1C, middle panel). This final condition was similar to the MTZ control, but all treatments differed from the polarized cortical actin observed in the Vh control group. Finally, trophozoites treated with both active principles did not show the presence of various typical actin structures, such as: filopodia, lamellipodia, adhesion plates, phagocytic mouths or stress fibers, unlike the control with Vh, which suggests immobility of parasites (Figure S1C, middle panel). These alterations were evidenced by TEM data and suggested that there are ultrastructural modifications on *E. histolytica* (Figure S1C). Trophozoites treated with MTZ, KP, or LL under the same dose conditions showed a reduction in the size and number of vacuoles, as well as a rearrangement of euchromatin, an increase in glycogen granules, and the presence of membranous structures such as autophagosomes or apoptotic bodies, arranged in the nuclear and vacuolar cavity, as well as the cytoplasm, compared to the Vh group (Figure S1C, lower panel).

2.3. Effect of Treatment with Active Principles KP and LL in ALA Model in M. auratus

The amoebicidal effect of KP and LL against ALA has been studied in hamsters [17–24]. The animals did not present a crisis episode associated with any behavioral change (such as: agitation, tremor, asthenia, anorexia, among others), symptoms of intoxication (such as: dyspnea, photophobia, blindness, diarrhea, tachycardia-arrhythmias, dystonia, myasthenia, seizures, epithelial pigmentation, among others), or anasarca (related to congestive heart failure, liver failure, or kidney failure) after 24 h of treatment. The hamsters did not show jaundice, pruritus or chills. However, body temperature was not be recorded to adequately rule out a febrile episode. Additionally, rodents were weighed at all times during the trial, but no changes in body weight or significant differences were observed between the treated and untreated groups ($p \geq 0.05$, ANOVA) (Table 2; Figure S2A). Only the LL group showed a slight decrease of - 0.21% in body weight compared to the control (disease-free) group (Figure 2SA). Thus, clinical conditions associated with the progression of ALA were ruled out, such as anorexia due to general malaise (fever, chills or muscle stiffness), abdominal pain (due to distension) or cachexia (due to acute diarrhea and bleeding/mucous membranes) [25]. Likewise, the results obtained from the antiparasitic activity suggest that there are no significant differences in the body weight of the ALA model, in addition no sign of toxicity was observed in the body weight of the hamsters, showing 100% survival with the administration of the treatments (Table 2).

Table 2. Antiparasitic effect of KP and LL on the development of ALA.

***In vivo* studies: acute toxicity and ALA characteristics**				
Treatments	**Vh**	**MTZ**	**KP**	**LL**
Hamster weight (g)	91.9 ± 2.3	95.4 ± 5.1	93.5 ± 6	93.4 ± 7.2
Toxicity signs	None	None	None	None
Survivors (%)	100	100	100	100
ALA Weight (g)	1.23 ± 0.15	0.33 ± 0.32 *	0.86 ± 0.15 *	0.40 ± 0.20 *
ALA Volume (mm^3)	2.257 ± 523.7	528 ± 183.5 *	738 ± 150 *	562.3 ± 23.3 *
NMR (T_1/ T_2)	Intermediate intensity/ Hyperintense	Intermediate intensity/ Hypointense	Intermediate intensity/ Hypointense	Intermediate intensity/ Hypointense
Leukocyte infiltrate	++	-	+/-	+/-
Fibrosis	+	--	--	--

 doi:10.20944/preprints202407.0797.v1

In vivo studies: acute toxicity and ALA characteristics				
Treatments	**Vh**	**MTZ**	**KP**	**LL**
Liquid	++	-	+/-	-
Edges	Irregular and poorly defined	Regular and well defined	Irregular and poorly defined	Regular and well defined
Morphology	Loculated ovoid	Round	Ovoid	Loculated ovoid

The following symbols correspond to the biological activity of the samples: ++, very high; +, high; +/-, medium; -, low; and --, very low. T_1, longitudinal relaxation times; T_2, transverse relaxation times. Results show the mean ± SD of two biological replicates ($n = 5$). (*) $p \leq 0.05$ vs. vehicle (1X PBS, negative control), ANOVA. Metronidazole was used as positive control (antiparasitic reference).

2.4. Paraclinical Analysis of Post-Treatment Liver and Kidney Function

The effect of KP and LL was evaluated in the course of ALA development by biochemical and hematological determinations (Figure 2, Table S1) [26,27]. The results obtained to evaluate the nutritional status showed hypertriglyceridemia in all experimental groups with respect to the reference values (30-145 mg/dL), while the groups treated with Vh and KP showed higher levels compared to the disease-free group ($p \leq 0.05$, ANOVA-Tukey) (Table S1). Furthermore, elevated cholesterol values were observed in the Vh and KP groups of 163 ± 21 and 164 ± 43 mg/dL respectively, compared to the disease-free group ($p \leq 0.05$, ANOVA-Dunnett). It is important highlight that, these results did not show alterations with respect to the reference range (94-237 mg/dL), and these data correlate with what was previously reported [28,29]. Protein values regardless of treatment remained within the reference range (4-8.6 g/dL), and no alterations were observed when comparing the data with the group free of liver abscess (Figure 2A). It is essential to mention that hypertriglyceridemia could be related to a high-calorie diet with low protein content, as well as to severe liver dysfunction and hepatic damage of any kind [30,31]. While, hypocholesterolemia may be associated with the severity of ALA due to findings found with virulent strains of *E. histolytica* in other animal models [32]. Thus, hepatic and renal functions were evaluated to determine the disease progression, possible toxicity associated with each treatment and liver tissue damage as a result thereof (Figure S2C).

Parameters used to evaluate the liver profile were: gamma glutamyl-transpeptidase (GGT), albumin (AL), alkaline phosphatase (ALP), transaminases (AST and ALT), bilirubin (total and direct), according to recommendations of the National Academy of Clinical Biochemistry and the American Association for the Study of Liver Diseases [33]. With this purpose, it was observed that the serum values of: AL, ALP, and direct bilirubin (DB), were different from the reference data for hamsters in all groups and with some exceptions also for the disease-free group ($p \leq 0.05$, ANOVA-Dunnett) (Table S1).

Treatments that induced significative hypoalbuminemia, hyperphosphatasemia, hyperbilirubinemia, and hypoazotemia were the Vh group, followed by KP, MTZ, and LL respectively (Figure 2B). Specifically, in relation to liver damage, the study showed that groups with the greatest damage extent were Vh and MTZ ($p \leq 0.05$, ANOVA-Tukey). However, this liver damage was associated with the ALA development for the Vh group (mainly) and KP (to a lesser extent), while the damage present in groups of MTZ and LL appears to be more directly associated with the treatments themselves, due to the correlation among the histopathological (Figure S2C) and paraclinical findings (Figure 2B) ($p \leq 0.05$, ANOVA-Tukey). All these results were sustained based on values of hyperphosphatasemia and hypertransaminasemia (ALT mainly) observed in the assay, because they correlate with hepatocellular necrosis, and therefore indirectly with the ALA (Table S1).

The different groups presented lower values of both parameters compared to the Vh group ($p \leq 0.05$, ANOVA-Tukey); but with the exception of the LL group in AST was similar (163 ± 22 U/L) ($p > 0.05$, ANOVA-Dunnett) or the MTZ group in ALT whose value exceeded the reference range used in this study (135 ± 23 U/L) ($p > 0.05$, ANOVA-Dunnett) (Figure 2B). However, these liver parameters remained higher in all groups compared to the disease-free group (Figure 2B) due to active cell necrosis (chronic type) and lack of remission but with stable progression of ALA (Figure S2B). This

 doi:10.20944/preprints202407.0797.v1

statement was correlated with the serum concentration of some proteins synthesized in the liver, such as GGT and AL (Figure 2B); because several studies demonstrated that during the development of liver abscesses (such as pyogenic), the AL decreases, while the GGT increases, as occurred in our study (Table S1) [34].

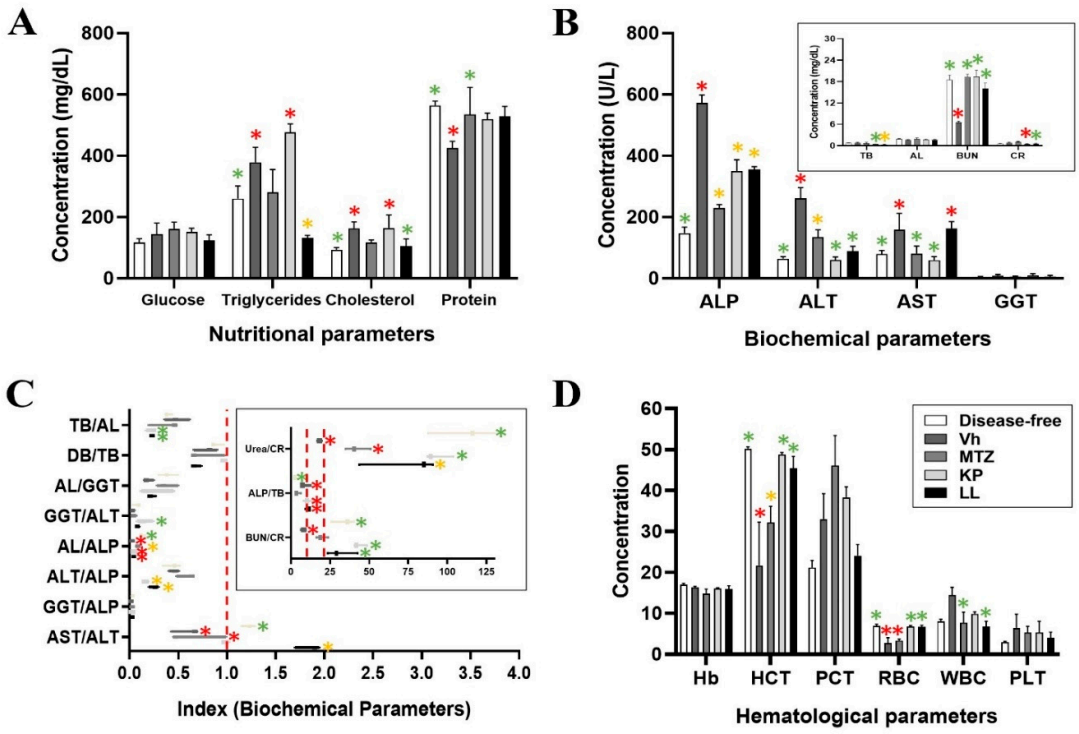

Figure 2. Paraclinical analyses of blood and serum from hamsters that developed ALA in the different treatment groups. Parameters analyzed were as follows: nutritional (**a**), biochemical (**b**), ratios (**c**), and hematological (**d**) (for details, see Table S1). Results show the mean ± S.D. (a, b, d) or the median and range (c) of two biological replicates (n = 5). * $p \leq 0.05$ vs. the control groups by ANOVA (red for disease-free; green for Vh; and yellow for both). Controls used in the study were MTZ such as positive control, Vh such as negative control (1X PBS, without treatment), and disease-free such as normal control (without ALA). Abbreviations used: ALP, alkaline phosphatase; ALT, alanine aminotransferase (GPT); AST, aspartate aminotransferase (GOT); GGT, gamma glutamyl-transpeptidase; TB, total bilirubin; AL, albumin; BUN, blood urea nitrogen; CR, creatinine; DB, direct bilirubin; Hb, hemoglobin (g/dL); HCT, hematocrit (%); PCT, plateletcrit (%); RBC, red blood cell (x10^6/mm^3); WBC, white blood cell (x100/mm^3); PLT, platelets (x10^6/µL).

Furthermore, it is relevant to mention that high values of TB, DB, GGT and ALP have been correlated with the size of ALA [35,39]. In this sense, the groups that presented the largest ALA size were Vh, followed by KP, MTZ and LL respectively ($p \leq 0.05$, ANOVA-Dunnett) (Figure 2B and Table 2). These results correlated with the histopathological findings observed (Figure S2C). At the same time, parameters such as transaminases, ALP and GGT have been related to hepatic obstruction (macro and micro), a common complication during ALA due to local necrosis and inflammation that can occur due to the pathology [39]. However, through paraclinical analysis it was not possible to demonstrate hepatic obstruction, unlike the histopathological analysis. This is because parameters such as GGT, cholesterol and TB, presented values (although high) within the limit range considered normal in this study. These parameters have been strongly associated with focal intrahepatic disease (such as ALA) by various authors [40–44]. There is a possibility that treatments with KP and LL could induce a period of metabolic compensation which later can maybe trigger complications associated with cholestasis. Still, studies with longer exposure time are necessary to clarify this possibility.

 doi:10.20944/preprints202407.0797.v1

On the other hand, the biochemical parameters of kidney function in the different treatments presented an inverse situation to that previously observed for liver function (Figure 2B). Comparisons made between the treatment groups with the study reference range demonstrated that urea values were lower than those found for the disease-free group (Table S1). Furthermore, the Vh group presented a considerable decrease in BUN values (6.5 ± 0.5 g/dL), while the MTZ group had a significant increase in creatinine (CR) values (1.01 ± 0.2 mg/dL), with respect to the group free of disease, for both cases ($p \leq 0.05$, ANOVA-Tukey) (Figure 2B). The hypoazotemia observed in the different treatment groups may be related to the inability of the liver to metabolize dietary proteins due to liver failure caused by ALA progression [45,46].

Therefore, it is possible to deduce that the Vh group presents less resolution of the ALA lesion, followed by the LL, KP, and MTZ group, respectively. However, the hypercreatinemia observed in the MTZ group may be associated with early renal dysfunction or acute renal failure due to complications related to the ALA and toxicity for the treatment itself [47,48]. Previous studies have shown that MTZ is eliminated renally and can accumulate in the body by altering glomerular filtration or tubular secretion [36]. This process can occur when some degree of renal failure is triggered and is known as a "drug-associated adverse event" [36], so it can additionally induce nephrotoxicity events during prolonged periods of administration.

To better understand liver and kidney function, different ratios were determined for each treatment group (Figure 2C) [38,40]. Ratios used to evaluate liver injury were AST/ALT, ALT/ALP, ALP/TB, and GGT/ALP [35–38]. The AST/ALT ratio (De Ritis ratio) was 1 ± 0.03 and 1.2 ± 0.07 for KP and disease-free respectively, which was associated with stable liver function; while MTZ and Vh presented a value < 1 related to hepatocellular damage (due to ALT elevation); whereas, LL showed a value > 1 possibly due to fibrosis, intrahepatic cholestasis or toxicity ($p \leq 0.05$, ANOVA-Dunnett) (Figure 2C) [38]. This result by biopsy and AST/PLT ratio index (APRI) was correlated to predict the degree of fibrosis among the groups (Figure 3B) [49]. However, the histopathological study did not show any alteration in the typical architecture of liver tissue associated with fibrosis. Also, the APRI value was < 0.5 in all groups and corroborated the absence of significant fibrosis on histopathology [50–52].

Additionally, the ALT/ALP ratio was lower in KP (0.17 ± 0.01) and LL (0.25 ± 0.05) compared to the other treatment groups ($p \leq 0.05$, ANOVA-Tukey) (Figure 2C). Commonly, low ALT/ALP values are associated with drug-induced intrahepatic cholestasis, mainly when there is a preferential increase of ALP over GGT (Table S1), as observed in this study [53]. In this sense, it is relevant to mention that the ALP/TB ratio was > 2 in all treatment groups compared to the disease-free group (2.23 ± 0.54) (Figure 2C). The ALP/TB and AST/ALT indices were used to predict the risk of fulminant liver failure associated with adjacent pathology of various etiologies (infectious and non-infectious) [54–56]. The groups that showed high ALP/TB values were LL (10.85 ± 1.28), KP (10.75 ± 3) and Vh (8.9 ± 2.9) ($p \leq 0.05$, ANOVA-Dunnett) (Figure 2C). But only LL also presented an elevation of the AST/ALT ratio, which reinforces the diagnosis proposed in this work [37]. Finally, the GGT/ALP ratio was < 5 in all groups, and the absence of obvious jaundice ruled out alcoholic liver disease (Figure 2C) [35,36].

Ratios used to predict the prognosis of ALA were AL/GGT, GGT/ALT, and AL/ALP [54–56]. The AL/GGT ratio was < 0.5 in all treatments, and they did not present significant differences among them ($p \geq 0.05$, ANOVA-Tukey) (Figure 2C). However, groups that showed a lower index concerning the disease-free group were KP (0.25 ± 0.18), LL (0.23 ± 0.038), and Vh (0.19 ± 0.05). These differences found in AL/GGT were due to decreased albumin values in the KP (1.7 ± 0.2 g/dL) and LL (1.7 ± 0.1 g/dL) groups (Table S1). It is relevant to mention that several investigations have demonstrated the predictive value of AL/GGT in various diseases [57].

 doi:10.20944/preprints202407.0797.v1

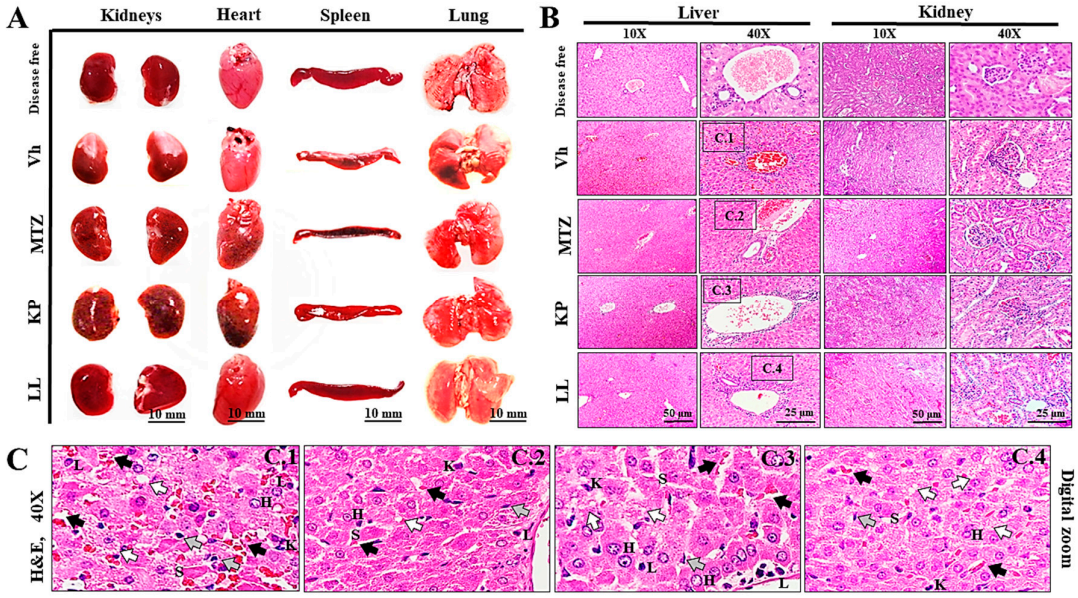

Figure 3. Histopathological analysis of organs extracted from hamsters with ALA of the different treatment groups. Anatomical morphology of the different body compartments: kidneys, heart, spleen and lungs, extracted from *M auratus* with ALA (**a**). Histopathological studies were performed on representative tissue sections of the liver and kidney stained with H&E shown at 10 to 40X magnification (**b**). Digital zoom with 40X magnification of histological sections of the liver from the different experimental groups to clearly visualize the following tissue architectures: hepatocytes (H), sinusoids (S), Kupffer cells (K), lymphocytes (L), focal intrahepatic cholestasis (gray arrow), bile canaliculi (black arrow) and lipid microvesicles (white arrow) (**c**). Representative results from two biological replicates (n = 5) are shown. MTZ was used as a positive control, Vh as a negative control, and disease-free status as a normal control.

However, the AL/GGT ratio should be taken with caution and interpreted solely based on liver function parameters and clinical correlation. Some studies with pyogenic liver abscesses demonstrated that low AL/GGT values are associated with a worse prognosis due to decreased AL and increased immunoglobulins [39]. This statement could contradict the results observed in this study. However, the low AL/GGT values in the KP and LL groups seem more related to liver or kidney dysfunctions due to the toxicity associated with the drugs themselves, according to the previous results of this study. Regarding the GGT/ALT ratio, a similar pattern was observed in all treatments, except in KP (0.15 ± 0.081), which showed a significant difference only with the Vh group (0.04 ± 0.01) ($p \leq 0.05$, ANOVA-Dunnett) (Figure 2C). Recently, several studies have begun to evaluate the predictive value of the GGT/ALT ratio during the treatment of diseases such as cancer and viral hepatitis [58,59]. In these studies, it was observed that an elevation of the GGT/ALT ratio was a predictor of poor prognosis for patients because GGT/ALT was associated with high rates of early recurrence and death from these diseases due to more aggressive forms, greater volume and extension of the disease, with frequent vascular invasion, as well as poor encapsulation, among others [60]. Although it is not common to use the GGT/ALT ratio for the prognosis of ALA, it is possible to predict that KP is a less effective treatment than LL or MTZ, although there were no statistically significant differences with the disease-free group ($p \geq 0.05$, ANOVA- Dunnett). While the AL/ALP ratio was < 0.1 in all treatment groups with respect to the disease-free control (0.13 ± 0.023) ($p \leq 0.05$, ANOVA-Dunnett) (Figure 2C). Only MTZ showed more similarity with the disease-free group, unlike KP and LL ($p \leq 0.05$, ANOVA-Tukey). The AL/ALP ratio has been used in oncology to assess disease progression [67]. To determine the ALA progression, it is not common to use the AL/ALP

 doi:10.20944/preprints202407.0797.v1

ratio; however, it is possible to predict that MTZ may be more effective in combating the disease than KP and LL.

The ratio used to determine the toxicity of the treatments was TB/AL [61–63]. The TB/AL ratio was lower in LL (0.22 ± 0.005) and KP (0.22 ± 0.04) ($p \leq 0.05$, ANOVA-Tukey), followed by the disease-free (0.40 ± 0.04) and MTZ (0.38 ± 0.16), compared to the group treated with Vh (0.48 ± 0.13) (Figure 2C). Various studies have highlighted the importance of the TB/LA ratio as a predictor of the risk of neurological damage in pathologies that induce the release of bilirubin into the bloodstream (hyperbilirubinemia), such as hepatitis, hepatocellular carcinoma, kernicterus, among others [64]. This is due to the toxicological effect that bilirubin induces on biological processes in the white matter of the brain [42]. The processes usually affected are the synthesis of macromolecules (DNA, RNA or proteins) and the uncoupling of oxidative phosphorylation, mainly in neurons, oligodendrocytes and astrocytes [65]. Elevated TB/AL values are more strongly associated with potential free (unconjugated or indirect) bilirubin neurotoxicity, placing the Vh group at greater risk than the other study treatments.

The ratios used to determine kidney damage or dysfunction were DB/TB, BUN/CR, and Urea/CR [66]. The DB/TB ratio was < 1 in all treatment groups and did not show significant differences among them ($p \geq 0.05$, ANOVA-Tukey) (Figure 2C). High values of DB/TB and CR are associated with renal failure in some pathologies, such as malaria caused by *Plasmodium falciparum* [59]. Although the DB/TB ratio does not apply specifically to ALA, neither group is at risk of developing hepatic or renal failure due to their similarities with the disease-free control. In this sense, the BUN/CR and Urea/CR ratios were used to find possible causes of sudden (acute) kidney problems [67].

In this study, it was observed that BUN/CR and Urea/CR ratios were < 10 and < 40 respectively, for the Vh group (7.9 ± 1.3 / 18.2 ± 1.35), which suggests intrinsic renal causes associated with liver disease like ALA ($p \leq 0.05$, ANOVA-Dunnett) (Figure 2C) [68,69]. Meanwhile, the same BUN/CR and Urea/CR ratios occurred in intervals of 10 to 20, and 40 to 110 for the MTZ group (19.6 ± 3.8 / 42 ± 8.15), which are associated with stable renal function or post-renal damage ($p \leq 0.05$, ANOVA-Dunnett) (Figure 2C) [68]. Therefore, these results do not adequately correlate with the preliminary findings presented in this acute renal failure study (Figure 3B), possibly because both BUN/CR and urea/CR values were within the upper limit of the considered normal range, for this study and the short duration of the treatments used in it [70]. Finally, the groups that presented a BUN/CR ratio > 25 were the KP (43.7 ± 4.3), LL (31.6 ± 9.8) and disease-free (34 ± 7.4) groups ($p \leq 0.05$, ANOVA-Dunnett) (Figure 2C), which are associated with prerenal causes such as dehydration, congestive heart failure, high protein consumption, among others [71].

Due to the similarity found in BUN/CR values of KP and LL, with the disease-free control group ($p \geq 0.05$, ANOVA-Tukey), it is possible to predict that the main cause is dehydration and rule out any other underlying pathology [72]. In this sense, the Urea/CR ratio was found within the normal range of 40 to 110 for KP (93.5 ± 9), LL (73.1 ± 26) and disease-free (112 ± 23) ($p \leq 0$ .05, ANOVA-Dunnett), which correlates with the result presented previously (Figure 2C) [73].

To conclude the paraclinical analyses, a complete blood count study was performed in the hamsters with ALA in the different treatment groups to evaluate the evolution and resolution of the disease (Figure 2D and Table S1). In the Vh group, moderate leukocytosis (19,600 ± 4,500/mm^3) of the leukemoid type was observed, without eosinophilia, and with the presence of anemia (3.5 ± 0.4 x10^6/mm^3) ($p \leq 0.05$, ANOVA-Tukey) (Figure 2D and Table 3). While the KP and LL groups did not present significant differences in their hematological parameters compared to the disease-free control group ($p \geq 0.05$, ANOVA-Dunnett) (Figure 2D). Only KP had a clinical picture of mild leukocytosis (14,800 ± 700/mm^3) compared to the LL or MTZ groups, according to the reference values used ($p \geq 0.05$, ANOVA-Tukey) (Figure 2D). The results obtained for KP and LL may be related to a remission of the disease [74]. In this sense, the neutrophil/lymphocyte ratio as a reliable predictor of systemic inflammation and poor prognosis associated with complications in pyogenic liver abscess was determined [75].

 doi:10.20944/preprints202407.0797.v1

Table 3. Hematic biometry of hamsters treated with ALA or KP or LL by manual differential analysis.

Treatments (%)	Disease-free	Vh	MTZ	KP	LL	Reference range (mean)
Lymphocytes	42 ± 4	**35 ± 13**	50 ± 13	**39 ± 12**	44 ± 21	40-85 (63)
Monocytes	0	0	0	0	0	1-6 (3)
Eosinophils	0	0	0	0	0	1-2
Basophils	0	0	0	0	0	0-5 (2)
Segmented neutrophils	54 ± 2	**64 ± 14**	51 ± 13	**60 ± 11**	**56 ± 21**	25-55 (40)
Band neutrophils	**4 ± 2**	**2 ± 1**	0	**2 ± 1**	0	5-13 (9)
Immature forms	0	0	0	0	0	0

Bold letters indicate differences with the reference range and **underlined** letters indicate higher values outside of this limit. Reference range, minimum and maximum normal value for the analyte of interest in hamster and the respective midrange [27,90]. Results show the mean ± SD of two biological replicates (n = 5). (*) $p \leq 0.05$ vs. Vh (1X PBS, negative control), ANOVA. MTZ was used as a positive control (antiparasitic reference).

Thus, the highest ratio of neutrophils/lymphocytes was for the Vh group (2.2 ± 1.4), followed by KP (1.67 ± 0.8), LL (1.66 ± 1.26), disease free (1.30 ± 0.15) and MTZ (1.15 ± 0.7), respectively. However, the similarities between the different treatment groups allow us to rule out possible serious inflammatory processes and sepsis ($p \geq 0.05$, ANOVA-Tukey). It is relevant to mention that the MTZ group also presented a clinical picture of moderate anemia similar to that observed for the Vh group, possibly due to side effects related to the treatment itself ($p \leq 0.05$, ANOVA-Dunnett) (Figure 2D) [76]. Other hematological parameters that tend to change during ALA, but did not show significant changes in this study, were Hb and PLT count (generally due to mild to severe thrombocytopenia, without obvious bleeding) ($p \geq 0.05$, ANOVA -Tukey) (Table S1) [77]. On the other hand, parameters not determined in this study and that can also be altered during ALA are those related to inflammatory processes such as erythrocyte sedimentation rate, C-reactive protein, prothrombin time and fibrinogen, which would be interesting perspectives to analyze and address in subsequent studies [78,79]

2.5. Treatments with LL and KP Were Effective in Inhibiting the Development of ALA in M. auratus.

The NMR images showed the localization, morphology and composition of ALA in the different groups (Figure S2B). In general, it was observed that the ALA in the left hepatic lobe of the animals showed marked differences in morphology (ranging from ovoid with defined edges to irregular), extension (localized or infiltrative to the abdominal cavity) and volume (500 to 2000 mm^3) (Table 2). However, most groups showed ovoid liver lesions, with regular and well-defined borders. The internal appearance was from hypointense (T_1) to heterogeneous (T_2) in various areas, which agrees with the classifications proposed by several authors. Elizondo *et al.* (1987) reported that untreated ALA is associated with an incomplete annulus (corresponding to an incomplete wall) and diffuse or wedge-shaped perilesional edema; but treated ALA, on the other hand, is associated with complete ring formation and edema returns to form concentric rings around the abscess (clinical type: subacute mild ALA) [80]. The above-mentioned characteristics match with the ultrasound sonographic classification proposed by N'Gbesso for the uncomplicated suppurative collection of ALA (type II) [81]. To highlight the fluid component in the liver collections as hyperintense signals, STIR sequence was used after removing the adipose tissue signal from the imaging study (Figure S2B). This sequence is relevant because the liquid content can be associated with inflammatory or liquefaction processes related to this pathology [82]. The order of hyperintense signals was the ALA group, followed by treatments with MTZ, KP and LL, in all cases related to disease progression (Figure S2B). Furthermore, MRI studies excluded common complications associated with the progression and dissemination of ALA to adjacent areas, such as pleural effusion, peritonitis, sepsis, subphrenic abscess, atelectasis, and pulmonary empyema [82]

 doi:10.20944/preprints202407.0797.v1

Imaging studies were correlated with anatomical morphology, and histopathological analyzes were performed on the livers removed postmortem and the ALA lesions recovered from them. At the time of the necropsy, the diaphragmatic side of the liver showed simple, single grayish lesions due to invasion of amoebic trophozoites. These lesions contained thick, odorless sterile material due to acellular proteinaceous debris from necrotic liver tissue, as described in other ALA studies [83]. However, the only study group that presented discrete hepatomegaly was the Vh group compared to the disease-free group ($p \leq 0.05$, ANOVA) (Table 2). The weight and dimensions of mice in the treatment groups were significantly lower than those in the Vh group (untreated) ($p \leq 0.05$, ANOVA) (Table 2 and Figure S2A). In the KP group, the ALA concentration decreased by 19.42%, while in the LL group it was 28.16%; these findings were similar to those of the MTZ group (antiparasitic reference drug) (Table 2).

Histological analysis of the liver collections revealed that the Vh group presented alterations in the architecture of the liver tissue due to granulomas (Figure S2C). These structures were of variable size, with necrotic-amorphous material inside possibly due to contact cytolysis, degradative enzymes such as proteases, phagocytosis and parasite resistance to host defense mechanisms [84]. Furthermore, capsule-shaped fibrosis, with compressed parenchyma, was delimited by amoebic trophozoites near the external wall of the ALA, similar to that reported by other authors [85]. Other characteristics observed were nonspecific periportal inflammation and the absence of amoebae within these areas (Figure S2C). Similarly, the inflammatory infiltrate was a mixture of types of neutrophilic leukocytosis characterized by the presence of lymphocytes, plasma cells, and segmented neutrophils, which correlated with blood count results (Table 3). On the other hand, the treatment groups exhibited similar histological characteristics, such as normal liver architecture but with vascular congestion, periportal inflammatory infiltrate and absence of amoebae within these areas (Figure S2C). Finally, the LL and MTZ groups also showed an increase in hemorrhagic-type zones in many sinusoid capillaries, characterized by an abundant content of red blood cells (Figure S2C). During the amoebic invasive process, trophozoites can induce an inflammatory response in the liver (as an underlying effect of the disease) [86]. This process was observed in all groups (Figure S2C). Moreover, the data suggest that KP and LL treatments have an antiamoebic effect similar to that of MTZ, possibly promoting regeneration around the liver injury, although the injury was not fully resolved. However, additional in-depth studies are needed to corroborate this claim.

2.6. Toxicological Evaluation of Hamsters Treated with KP or LL during ALA Treatment

Morphometric analysis of organs removed postmortem during necropsy was performed in ALA-treated hamsters to observe changes in weight and dimensions associated with the treatments after infection (Table 4). The organs did not show significant morphological changes during anatomical inspection compared to those of the control group (disease-free) at the end of each treatment ($p \geq 0.05$, ANOVA). The kidneys had the typical bean shape (with a convex area and other concave areas), with a capsule of whitish fibrous tissue interrupted at the level of the renal hilum, where the ureter and blood vessels are located (Figure 3A, kidneys). The heart was shaped like an inverted cone, with the apex directed to the left; four cavities separated by a septum (atria and ventricles); and at the base, the vena cava (superior, inferior and pulmonary) and other arteries (pulmonary and aortic) (Figure 3A, heart). The spleen was elongated, flat, thin and curved at the edges, with a splenic hilum, numerous blood vessels and a connective tissue capsule that gave off trabeculae inside (Figure 3A, spleen). The lungs were cone-shaped and divided into lobes. The lungs were located on the right and left within the thoracic cavity and showed some differences. The right lung (short and wide) had three lobes (upper, middle and lower) divided by a horizontal and an oblique fissure. The left lung had a single lobe (Figure 3A, lungs).

Additionally, histopathological studies of the liver and kidneys were performed to corroborate these results. Organs of the hamsters maintained a normal appearance with the integrity of their tissue structure, regardless of the treatment administered in all groups, as did those of the disease-free group (Figure 3B). Mainly, the livers had a stroma of fibrous connective tissue and a parenchyma with numerous hepatocytes grouped in cell sheets. The liver lobes were not visible and the central

 doi:10.20944/preprints202407.0797.v1

veins had a large diameter (Figure 3B, livers at 10X). Additionally, portal spaces were observed between nearby lobes, formed by portal triads with a portal vein, a hepatic artery, and a bile duct (Figure 3B, liver at 40X). These characteristics were consistent with those reported in the literature [87–90]; apparently, the liver tissue did not show any noticeable damage or change, except for those previously noted for this organ. However, hepatocytes of variable size and some eosinophilic (glycogenic) cells were observed that were arranged in cords of two or more cells separated by sinusoids; all of these features are consistent with areas of possible regeneration (Figure 3C, letter H). Furthermore, the samples presented sinusoids lined with endothelial cells (Figure 3C, letter S) but with numerous Kupffer cells (Figure 3C, letter K), lymphocytes (Figure 3C, letter L) and vascular congestion associated with inflammatory and focal intrahepatic infiltrates. Subacute type cholestasis (Figure 3C, gray arrow) due to the accumulation of discrete bile plugs in the bile canaliculi (Figure 3C, black arrow) was also observed.

On the other hand, the kidneys had a capsule, a cortex, a medulla with numerous medullary pyramids, and a calyx. Likewise, many nephrons were observed, with a renal corpuscle and numerous tubules (Figure 3B, kidneys at 10X). In turn, the glomeruli presented a proximal convoluted tubule, capsule of Bowman, mesangial matrix, urinary space, capillary lumens, arterioles, and distal convoluted tubule (Figure 3B, kidneys at 40X). Similarly, the renal tissue did not show visible damage or relevant changes in its tissue architecture, with some exceptions for the Vh and MTZ groups. Finally, all these results suggest that KP and LL administrated in short times do not induce important tissue damage in liver or kidneys. Several studies have shown the safety of multiple polyphenolics and terpenoids compounds coming from natural sources. However, each polyphenol or terpene used in medicinal applications should be studied carefully to determine its potential acute or chronic harmful effects.

Table 4. Morphometric analysis of organs extracted from hamsters treated with ALA or KP or LL.

Organs	Disease-free	Vh	MTZ	KP	LL
Liver	6.7 ± 0.07/4.04 ± 0.05	**8.28 ± 1.1*/4.7 ± 0.5***	5.76 ± 1.4/4 ± 0.15	5.9 ± 0.8/3.88 ± 0.11	5.5 ± 0.9/3.94 ± 0.16
Heart	0.4 ± 0.0/0.8 ± 0.09	0.38 ± 0.05/1.06 ± 0.09	0.38 ± 0.1/1.08 ± 0.04	0.38 ± 0.1/1.06 ± 0.08	0.38 ± 0.08/1.1 ± 0.07
Kidneys	0.65 ± 0.07/1.2 ± 0.14	0.62 ± 0.03/1.2 ± 0.07	0.52 ± 0.0/1.3 ± 0.08	0.49 ± 0.04/1.2 ± 0.1	0.49 ± 0.07/1.1 ± 0.08
Lungs	0.67 ± 0.0/2.8 ± 0.2	0.7 ± 0.05/2.6 ± 0.2	0.68 ± 0.05/2.5 ± 0.2	0.74 ± 0.06/2.5 ± 0.05	0.74 ± 0.06/2.4 ± 0.1
Spleen	0.2 ± 0.0/3.4 ± 0.38	0.2 ± 0.0/3.30 ± 0.4	0.2 ± 0.05/3.3 ± 0.3	0.36 ± 0.05/3.7 ± 0.1	0.26 ± 0.05/3.4 ± 0.4

Measurement of weight (g) / larger diameter (cm) for each organ in the different treatment groups. **Bold letters** indicate significant differences with respect to the disease-free group. Results show the mean ± SD of two biological replicates (n = 5). (*) $p \leq 0.05$ vs. Vh (1X PBS, negative control), ANOVA. MTZ was used as a positive control (antiparasitic reference).

2.7. In Silico Analyses to Determine the Toxicity of KP and LL

Bioinformatics studies were also conducted with KP and LL to determine whether they had: *i*) pharmacological properties similar to those of antiprotozoal drugs commonly used against amoebiasis (such as MTZ), *ii)* possible adverse effects during treatment in an animal model, and *iii)* potential molecular targets of both compounds. These analyses revealed that KP and LL meet the criteria proposed by diverse drug-likeness models based on the physicochemical properties of both compounds (Figure 4 and Table 5), as follows: Lipinski (*log P*: ≤ 5, MW: ≤ 500 Da, HBA: ≤ 10, and HBD: ≤ 5) [39]; Ghose (*log P*: -0.4 to +5.6, MR: 40 to 130, MW: 180 to 480 Da, and A: 20 to 70) [40]; Veber (RB: ≤ 10, and PSA: ≤ 140 Å2) [41]; Egan (*log P*: ≤ 5.88, and PSA: ≤ 131.6) [42]; or Muegge (MW: 200 to 600 Da, *Log P*: -2 to +5, PSA: ≤ 150, R: ≤ 7, C: > 4, HA: > 1, RB: ≤ 15, HBA: ≤ 10, and HBD: ≤ 5) [43].

 doi:10.20944/preprints202407.0797.v1

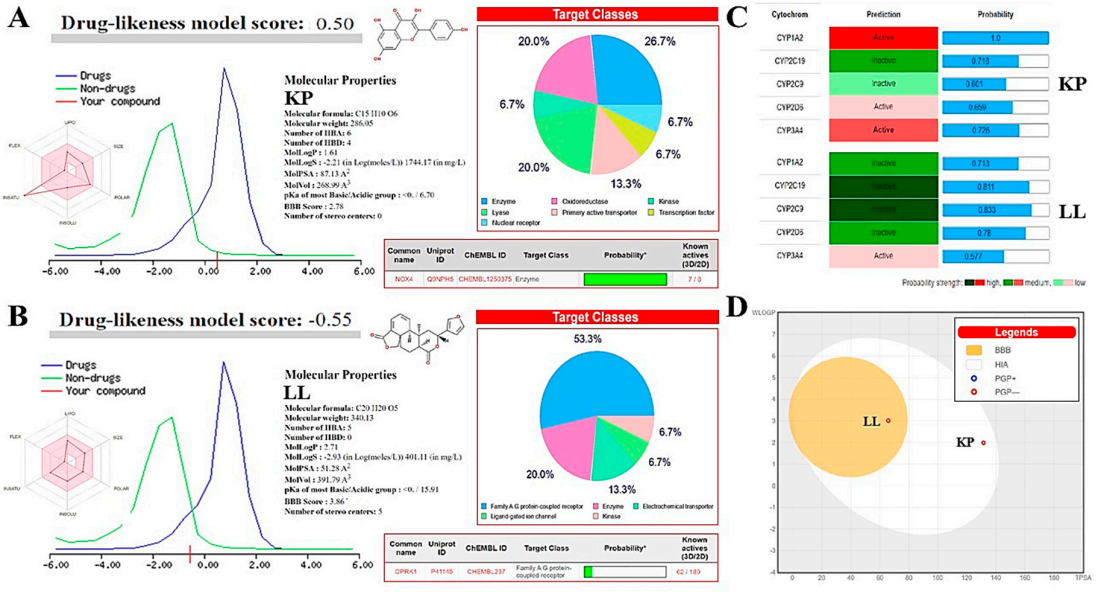

Figure 4. Predictions of the pharmacokinetics, toxicity and molecular targets of KP and LL based on their physicochemical properties. The molecular properties and chemical structures of KP (a) and LL (b) were used to predict similarities with biologically active drugs through the Molsoft© drug similarity model and their potential target pharmacophores using SIB© SwissTarget prediction. (c) The toxicological activity of both active principles, similar to antiparasitic drugs in humans, was predicted through inhibitory effects on the enzyme complex associated with CYP using a predictive machine learning model based on specific fingerprints called MCF with SuperCYPsPred of Structural Bioinformatics©. (d) Other toxicity characteristics, such as BBB permeability, HIA, and PGP affinity, were predicted by the SIB© SwissADME boiled egg permeation method. Results were compared with MTZ, an amoebicidal compound used to treatment of diverse parasitic diseases (see supplementary material). Abbreviations used: MCF, most common features; BBB, blood-brain barrier; HIA, health impact assessment; PGP, *P*-glycoprotein; BOILED, brain or intestinal estimated; ADME, absorption, distribution, metabolism and excretion; CYP, cytochrome-P450 system; HBA, hydrogen bond acceptors; HBD, hydrogen bond donors; *Log P*, partition coefficient; *Log S*, aqueous solubility coefficient; *pKa*, acid dissociation coefficient; PSA, polar surface area; LIPO, lipophilicity; POLAR, polarity; INSOLU, insolubility; INSATU, insaturation; FLEX, flexibility, NOX4, NADPH oxidase IV; OPRK, Kappa Opioid receptor.

The main physicochemical properties observed in KP were low flexibility and high unsaturation, medium polarity (*Log P*: 1.61) with water solubility of 2.60 x10^{-4} mol/L and high passive absorption through the gastrointestinal tract (PSA: 87.13 A^2 in CACO- 2) (Figure 4A); while LL showed low flexibility, intermediate lipophilicity (*Log P*: 2.73) with a water solubility of 1.33 x10^{-4} mol/L, as well as high gastrointestinal absorption (PSA: 51.28 A^2 in CACO-2) and permeability passive across the blood-brain barrier (BBB score: 3.86) (Figure 4B). In both cases, the compounds have a high probability of being bioavailable at biological pH in rats (> 10%, *F* = 0.55 based on PSA values), and neither molecule appears to be permeable to the skin or eliminated from the central nervous system by *P*-glycoprotein (*P*-gp) (Figure 4D). It is relevant to mention that *P*-gp is known as multidrug resistance protein-1 (MDR1 or ABCB1), and is abundant in the intestinal epithelium, liver, kidneys, blood-brain and blood-testicular barriers, as well as some tumors [43]. Therefore, KP and LL may be active against different types of tumors, but more in-depth studies are necessary to explore this possibility.

The Drug-Likeness Model of Molsoft© (DLMS) predicted that KP (DLMS: 0.5, high) is a compound most similar to a drug compared to LL (DLMS: -0.55, low) (Figure 4A and B), as well as higher bioactive potential respect to the MTZ control (DLMS: 0.24, medium) (Figure S3). Possibly, LL had a low score due to the toxicity prediction associated with its molecular structure (ToxiM: 0.958)

 doi:10.20944/preprints202407.0797.v1

and structural alarm of Brenk (> 2 esters) (Table 5). However, experimental results showed that LL had the higher selectivity in its biological effect compared to KP by different methods (Table 5 and Figure 4). Therefore, DLMS results should be taken with caution and confirmed by the animal model to clarify this doubt.

Table 5. Bioinformatic analysis of pharmacological and toxicological properties of KP and LL.

Samples	MTZ	KP	LL
SwissADME©: Physicochemical Properties			
Density:	1.5±0.1 g/cm^3	1.7±0.1 g/cm^3	1.3±0.1 g/cm^3
Refraction index:	1.612	1.785	1.612
Polarizability:	16.2 ± 0.5 10^{-24}cm^3	28.3 ± 0.5 10^{-24}cm^3	35.0 ± 0.5 10^{-24}cm^3
Surface tension:	60.5 ± 7.0 dyne/cm	98.9 ± 3.0 dyne/cm	54.6 ± 5.0 dyne/cm
No. heavy atoms:	12	21	25
No. of bonds:	12	23	29
No. of rings:	1	3	5
No. aromatic heavy atoms:	5	16	5
Fraction Csp3:	0.50	0.00	0.50
No. rotatable bonds:	3	1	1
Total charge:	0.0	0.0	0.0
Molar refractivity:	43.25 Å	76.01 Å	88.42 Å
SwissADME©: Pharmacokinetics/Molinspiration©: Bioactivity score			
GI absorption:	High	High	High
P-gp substrate:	No	No	No
Log *Kp*:	-7.36 cm/s	-6.70 cm/s	-6.37 cm/s
GPCR ligand:	- 1.09	- 0.10	**0.65**
Ion channel modulator:	- 0.87	- 0.21	**0.16**
Kinase inhibitor:	- 0.59	**0.21**	- 0.13
Nuclear receptor ligand:	- 1.74	**0.32**	**0.66**
Protease inhibitor:	- 1.68	- 0.27	0.04
Enzyme inhibitor:	- 0.32	**0.26**	**0.47**
SwissADME©: Medicinal Chemistry			
PAINS:	0 alert	**1 alert (catechol A)**	0 alert
Brenk:	**2 alerts (Nitro group)**	**1 alert (catechol A)**	**1 alert (> 2 esters)**
Leadlikeness:	**No (M.W. < 250)**	Yes	Yes
Synthetic accessibility:	2.30	3.14	5.56
T.E.S.T.© and LAZAR©: Toxicological properties			
LD$_{50}$ *Fathead minnow* (96 h):	424.1 mg/L	1.28 mg/L	ND
LD$_{50}$ *Daphnia magna* (48 h):	39.14 mg/L	3.62 mg/L	ND
IGC$_{50}$ *T. pyriformis* (48 h):	270.22	10.54 mg/L	ND
LD$_{50}$ Rat (Oral):	2,444	2,018 mg/kg	ND
Bioconcentration factor:	1.914	**8.032**	ND
Developmental toxicity:	Not	**Yes**	ND
AMES mutagenicity:	**Yes (p = 0.67)**	**Yes (p = 0.42)**	ND
Carcinogenicity (rodents):	ND	No (p = 0.43)	ND
Adverse effects (rat)	ND	1,320 mg/kg/day	ND
Estrogen Receptor RBA:	5.089 10^{-4}	0.004	ND
Estrogen Receptor Binding:	**Yes**	**Yes**	ND

The results shown in bold are out-of-range values. ND, not determined. Abbreviations used: ADME, absorption, distribution, metabolism, and excretion; GI, gastrointestinal; *P*-gp, *P*-glycoprotein; *Log Kp*, human skin permeability coefficients; GPCR, G protein-coupled receptor; PAINS, pan assay interference structures; Brenk, structural alert; LD$_{50}$, median lethal dose; IGC$_{50}$, half-maximal inhibition growth concentration; RBA, relative binding affinity. MTZ was used as positive control (antiparasitic reference).

 doi:10.20944/preprints202407.0797.v1

Results predicting biological activity in humans indicate that KP may act as a kinase inhibitor and nuclear receptor ligand, while LL may act as a ligand of G protein-coupled receptors (GPCRs) or nuclear receptor ligand and modulate ion channels (Figure 4). Among the most likely pharmacophore targets for KP and LL are NADPH oxidase-IV (NOX4) and kappa-opioid receptor (OPRK1) (Table S2 and S3), respectively. NOX4 is mainly expressed in the kidney, and its function is to produce hydrogen peroxide (H_2O_2) [44]; while OPRK1 is a receptor for opioid-like compounds in the brain, and its function is to regulate the effects of these compounds (such as alteration of nociception, consciousness, motor control, and mood) [45]. These findings are important because they allow for predicting anti-inflammatory properties for KP and sedative effects for LL, as well as the possible harmful effects of both compounds on human health and their probable antiparasitic mechanism against *E. histolytica*.

Several studies have shown that *E. histolytica* has homologous proteins similar to those mentioned, and these proteins have significant functions in the biology of this parasite, as presented below: The amoeba contains a significant amount of kinase enzymes that regulate various functions such as cell signaling, metabolism, cell division, and survival [46]; nuclear receptors which are transcription factors that regulate the response of small lipophilic compounds, play a crucial role in human development, physiology and disease [45]; signaling pathways associated with G-proteins are factors that contribute to the pathogenesis of this protozoan, by modulating amoebic motility through the regulation of the dynamic actin cytoskeleton, among other cellular processes. These processes include migration, vesicular trafficking in phagocytosis, secretion of virulence factors, invasion, evasion of host immune response, and binding-killing of host cells [46,47]; ion channels are membrane proteins that regulate ions such as Ca^{+2}. In *E. histolytica* these channels have cytopathic activity and play a role in growth and differentiation [48]. However, complementary studies are necessary to confirm the role of these proteins in the amoebicidal action mechanisms of KP and LL. For instance, comparative studies with orthologous proteins from other amoebae (pathogenic and non-pathogenic) and their homologs in *Homo sapiens* are needed.

3. Materials and Methods

3.1. Isolation and Purification of Active Principles KP and LL

Using chromatography and NMR, the active principles KP (tetrahydroxyflavone) and LL (diterpene) were isolated, purified, and characterized, with a purity of ≥ 95% using the previously reported method [9,10]. MTZ was used as antiparasitic reference in the different assays and acquired from Liomont Infinitely© Pharm. (Flagenase 400®).

3.2. Cell Cultures

Cell lines were acquired from ATCC® (Manassas, Virginia, U.S.), maintained in 80% confluence, and harvested in the log phase of growth for all experiments. Cell lines transformed/non-tumorigenic used were: Chinese hamster ovarian epithelium (CHO-K1, CCL-61™) and human lung/bronchial epithelium (BEAS-2B, CRL-9609™). *E. histolytica* trophozoites (HM-1: IMSS, 30459™) were axenically cultivated in microaerophilic conditions and virulence was maintained through successive passages into liver of hamsters [4,5]. All cell lines were cultured and maintained according to the manufacturer's instructions [12,14]. Cell density at collection time was determined by Trypan blue stain (0.4%, Sigma®). Finally, cell viability, half-maximal inhibitory concentration (IC_{50}), selectivity index (SI), and Median lethal dose (LD_{50}), were calculated as follow [73]: *% Viability = (Abs_{sample} / $Abs_{control}$) * 100; IC_{50} was obtained by regression analysis (percent survival vs. log concentration); SI = IC_{50} normal cell line / IC_{50} trophozoites cell line; LD_{50} (oral, mg/kg) = 10^X [(0.372 * log IC_{50} normal cell line) + 2.024].*

3.3. Cytotoxicity Assays in Normal Cell Lines by Formazan Salts

BEAS-2B and CHO-K1 were used to evaluate the cytotoxic effect of KP and LL with the MTT assay [24]. Cells (20 x10^3 cells/per well) were placed in 96-well microplates (Corning®) with 200 µL of supplemented medium for 24 h. Cells were treated with KP, LL, MTZ (10 to 500 µg/ml), and 1 X

 doi:10.20944/preprints202407.0797.v1

PBS (vehicle; Vh) for 24 h under the same conditions. Four hours before ending the treatments, 20 µL of MTT (5 mg/mL in 1X PBS, Sigma®) was added. Subsequently, the supernatant was removed and the formazan was dissolved in 200 µL of acidified isopropyl alcohol (0.2% HCl, J.T. Baker®). Cell viability was determined at λ 590 nm in a microplate reader (model 680, Bio-Rad®) [25,26].

3.4. Cell Death Determination by Flow Cytometry

Based on the previously reported IC_{50} [26], the trophozoites (1 x10^5/mL) were cultivated and treated in presence of compounds for 48 h. The treatments were MTZ (0.08, 0.16 µg/mL), KP (15.8, 31.6 µg/mL), LL (15.6 µg/mL), and Vh (1X PBS). Then, trophozoites were resuspended in 500 µL of 1X binding buffer and stained with 5 µL of AnV-FITC and PI (K109, Biovin®) for 10 min at 37°C. Samples were processed by flow cytometry on a BD FACS-Calibur™ (Becton Dickinson®) and 20 x10^3 events were read at $\lambda_{ex/em}$ 485/538 nm (AnV-FITC) and $\lambda_{ex/em}$ 538/620 nm (PI). The obtained data (size, granularity and fluorescence) were analyzed with Flowing Software (version 2.5.1; Turku University) and simultaneously corroborated by confocal microscopy (LSM-700; Zeiss®) with a magnification of 40X [12].

3.5. Cell Morphology by Confocal Microscopy

Trophozoites (1 x10^5/ml) were incubated with the IC_{50} for 1 h at 37°C (KP: 7.9 µg/mL; LL: 7.8 µg/mL; MTZ: 0.04 µg/mL; 1X PBS), with culture medium supplemented with serum on previously sterilized coverslips [9,10]. The culture medium was removed and the adhered cells were fixed with 4% paraformaldehyde for 1 h at 37°C. Samples were washed three times with 1X PBS and incubated with 1:50 Rhodamine-phalloidin (R415, Invitrogen®) for 1 h at 37°C. Finally, the cells were washed and mounted with Vecta Shield®/DAPI medium (Vector Laboratories®), to finally be observed using a confocal microscope (LSM-700, Zeiss®) [12].

3.6. Ultrastructural Morphology Analysis via Transmission Electron Microscopy (TEM)

Trophozoites were treated with the IC_{50} of KP and LL for 48 h at 37°C. Subsequently, they were harvested and processed according to the method reported [48]. Trophozoites were fixed with 2.5% glutaraldehyde (Sigma®) in sodium cacodylate buffer (0.1 M, pH 7.2) for 24 h at 25°C. Post-fixation was then performed with 1% osmium tetroxide (Sigma®) for 1 h at 25°C. Samples were dehydrated with ethanol: propylene oxide (Sigma®) (50, 70, 90, 100% EtOH) for 10 min at 4°C and placed in polymerized epoxy resin (Poly/Bed® 812, Polysciences®) at 60°C for 24 h. Ultrathin sections of 60 nm thickness were obtained with an ultramicrotome (Porter-Blum MT-1, Sorvall®), and were stained with 2% uranyl acetate (Polyscienc-es®) for 20 min and 0.2% lead citrate. (Polysciences®) for 5 min. Finally, the samples were observed in TEM (JEM-1011, JEOL®) [12].

3.7. ALA Model in Hamster

For this study, *M. auratus* (Syrian hamster) was used as animal model because the hamster is naturally susceptible to infection by *E. histolytica* and can develop amoebic colitis or extraintestinal complications such as ALA. Animals were provided by the animal production and experimentation unit (UPEAL-CINVESTAV), following the 2011 version of the Mexican Standard (NOM-062-ZOO-1999; approved protocol number 0183-16). This study was carried out according to the protocol NC3Rs ARRIVE (See Appendix A, NC3Rs ARRIVE Guidelines Checklist). Male golden hamsters (sexually mature and homozygous) were selected with 95 ± 5 g of body weight, and ≈ 10 weeks old. Animals were maintained in aseptic conditions at 25 ± 1°C, 50 ± 3% humidity, with 12 h light-dark cycles and *ad libitum* access to standard diet (LabDiet®) and water (Figure 5A).

Four experimental groups were formed with five animals each, based on OECD rules. Laparotomy was performed under aseptic conditions, and virulent *E. histolytica* trophozoites (1.5 x10^6) were inoculated into the left hepatic lobe by intrahepatic puncture in 100 µL of 1X PBS to ALA induction [50]. The development of hepatic lesion for ALA was monitored for 4 days. Antiparasitic activity protocol started with the administration of treatments to the fourth day post-infection, i.p.

 doi:10.20944/preprints202407.0797.v1

route, daily every 24 h for 4 days, to favor greater bioavailability in the experimental model. The optimal doses of KP and LL were determined based on previous cytotoxic studies, bioinformatic analysis, and the doses of MTZ used in humans. Doses used were 5 mg/kg of body weight to KP and 10 mg/kg of body weight to LL [51]. Controls used were MTZ (antiamoebic control) at 10 mg/kg body weight and 200 µL of 1X PBS (Vh control) Finally, biological samples of blood, organs and abscesses were obtained post-mortem (Figure 5B) [31–35].

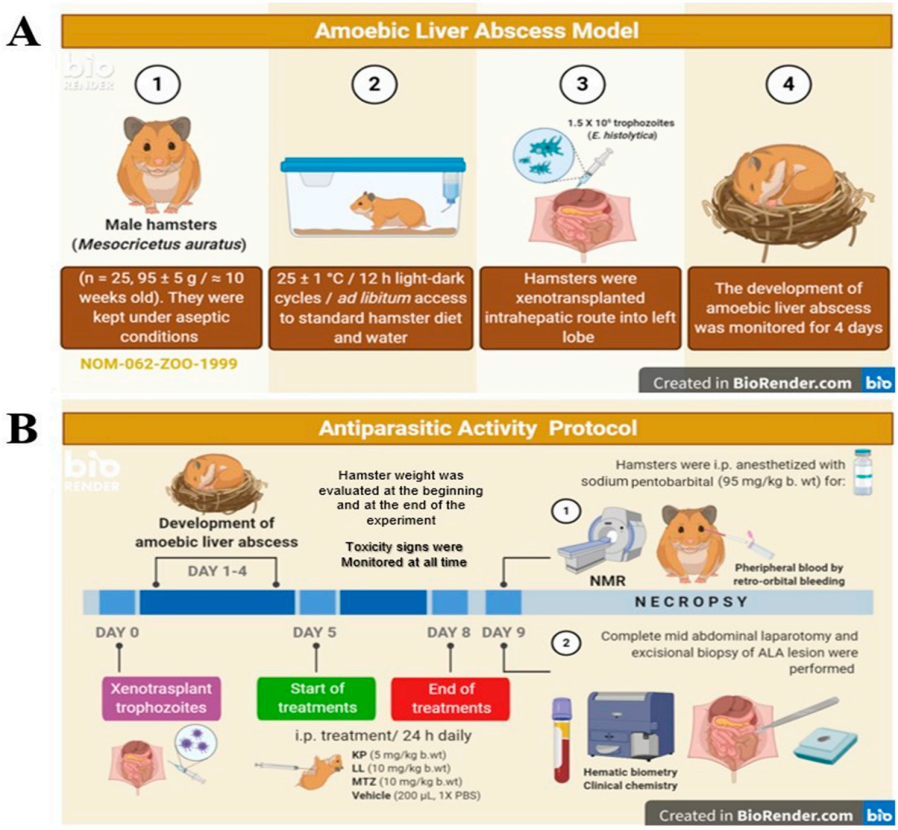

Figure 5. Timeline of the antiparasitic protocol implemented for KP and LL. The antiprotozoal activity of KP and LL was determined in *E. histolytica* trophozoites xenotransplanted into livers from male *Mesocricetus auratus* (Syrian hamster), according to the protocol proposed by Tsutsumi *et al*. 1984 and the Official Mexican Regulations (NOM-062-ZOO-1999).

3.8. Imaging Magnetic Resonance (NMR)

NMR analysis was performed using MAGNETOM Symphony™ with a Tim 1.5 Techo system (Siemens Medical Solutions™, Germany), with a human knee diagnostic antenna without paramagnetic contrast. Animals were previously processed and placed in supine and craneocaudal positions. The sequences/parameters used were: coronal projections T_1 (thickness of cut: 1.5 mm; TR/TE: 500/20 ms; field of view: 130 mm; matrix: 512), T_2 (thickness of cut: 2 mm; TR/TE: 3890/117 ms; field of view: 180 mm; matrix: 512) and STIR (thickness of cut: 3 mm; TR/TE/TI: 5000 ms/29 ms/130 ms; field of view: 153 mm; matrix: 512). After imaging studies, results were analyzed in the RadiAnt DICOM Viewer software (v3.4, Medixant©), to perform the measurement and characterization of ALA lesions, as well as 3D reconstructions.

3.9. Paraclinical Analysis

Peripheral blood samples were obtained by retro-orbital puncture in anesthetized animals using heparinized capillary tubes (Vitrex®) and collected in pediatric tubes with K_2EDTA (BD Microtainer®) for hematic biometry or without anticoagulant for chemical sanguineous (BD

 doi:10.20944/preprints202407.0797.v1

Microtainer®). Serum was obtained by centrifugation at 3,500 rpm and frozen at -70°C until the clinical analysis time. Hematic biometry was performed in hematology autoanalyzer system (BC-2300, Mindray®) and biochemical parameters was made on automatic medical system (Prestige® 24i, Tokyo Boeki®).

3.10. Histopathological Analysis

After blood samples were obtained, hamsters were sacrificed with excess anesthesia and cervical fracture for mounted on a dissecting board to make the necropsy. A complete mid-laparotomy was performed for the dissection of lungs, spleen, heart, liver, and kidneys. Excisional biopsy was made to recovery ALA lesion for morphometric analysis. Organs and ALA lesion were rinsed with 1X PBS, weighted and adherent tissue removed. Subsequently, samples were fixed in 4% paraformaldehyde (Sigma®) and stored at 4°C for 48 h. Later, inclusion protocol was performed to obtain histological sections of 3 μm thickness with a rotatory microtome (RM2125-RTS, Leica®). Tissue slices were stained with hematoxylin-eosin (Merck®), mounted on coverslips with Entellan™-New (Merck®), and observed by optical microscopy (Eclipse 80i, Nikon®).

3.11. In Silico Analyses

The chemical structures, molecular properties, and SMILES notations of the compounds were obtained by ChemSketch™ (v1 2.0, ACD®). SMILES notations from KP and LL were fed into SwissDrugDesign© applications (Swiss Institute of Bioinformatics©, CH) (https://www.molecular-modelling.ch/swiss-drug-design.html), such as *i*) SwissADME (v2019, SIB©), to create predictive models for the physicochemical properties, pharmacokinetics, drug likeness, and medicinal chemistry friendliness of multiple molecules [37]; and *ii*) SwissTargetPrediction (v2017, SIB©), to predict possible targets of bioactive small molecules in humans and other vertebrates [38]. Additionally, to complement and validate the data provided for SwissDrugDesign©, the following online bioinformatic programs were used: *i*) Molsoft Drug-Likeness model (Molsoft©, U.S.) (http://molsoft.com/mprop/); *ii*) Molinspiration© (v2018.10, Molinspiration Cheminformatics©, S.K.) (www.molinspiration.com); and *iii*) ToxiM (IISER©, IN.) (http://metagenomics.iiserb.ac.in/ToxiM/index.html) [39]; *iv*) T.E.S.T. (v4.1, U.S. EPA) (https://comptox.epa.gov/dashboard/predictions/index) [40]; *v*) Toxtree (v3.1.0, Ideaconsult Ltd) (http://toxtree.sourceforge.net/); *vi*) SuperCYPsPred (v2020, Structural Bioinformatics©) (http://insilico-cyp.charite.de/SuperCYPsPred/index.php?site=home) [60]; vii) LAZAR (v1.4.2, IST-gmbh©) (https://lazar.in-silico.ch/predict) [41,42].

3.12. Statistical Analysis

Results were presented as follows: *i*) for *in vitro* studies, as mean ± standard deviation (S.D.) of three independent assays performed for triplicate ($n = 9$); and *ii*) for *in vivo* studies, as mean ± S.D. of two biological replicates ($n = 5$). Other descriptive statistics used such as median and range, were specified in the text or figure. Additionally, normality and outlier tests were performed with Anderson-Darling and Grubbs, respectively. Results were analyzed with *t*-Student or one-way ANOVA (for parametric data with normal distribution), and means were compared with normal/pathological controls through the post hoc test of Tukey-Kramer or Dunnett, by Minitab 18 statistical software (v18.1.0, Minitab®), and GraphPad Prism® (v8.0.2, GraphPad©). Differences found in all statistical tests were considered significant when $p \leq 0.05$ (*) or 0.01 (***).

4. Conclusions

The results of the study demonstrated the antiparasitic effects of KP and LL on *E. histolytica* trophozoites through a decrease in cell viability, alterations in mobility and morphological changes associated with cell death by apoptosis, changes in the actin cytoskeleton and cell arrest, respectively. However, these effects were not very selective and *E. histolytica* was more sensitive to LL than to KP. Bioinformatic predictions showed that KP could act as a kinase inhibitor and nuclear receptor ligand,

 doi:10.20944/preprints202407.0797.v1

while LL could be a GPCR ligand and modulate ion channels. Among the most likely pharmacophore targets for KP and LL are NOX4 and OPRK1, respectively. Both targets are widely present in eukaryotic organisms. Therefore, KP and LL may have potential anti-inflammatory and sedative effects, but additional studies are needed to clarify this possibility. Furthermore, KP and LL had antiparasitic effects in hamsters infected with *E. histolytica* trophozoites. This effect was evidenced by the reduction of ALA lesions, and was corroborated by imaging/histopathological studies. However, KP was less effective than LL, but toxicological studies have shown that LL treatment is more toxic than KP treatment. Both active substances induced intrahepatic cholestasis, but LL could increase the risk of liver failure. These findings demonstrated the therapeutic potential of both molecules against antiparasitic diseases related to *E. histolytica*, but additional in-depth studies are necessary to understand their possible harmful effects on human health and their antiparasitic mechanism.

Supplementary Materials: The following supporting information can be downloaded at the website of this paper posted on Preprints.org. Figure S1: Biological activity of KP and LL in trophozoites. Figure S2: Antiamoebic activity of KP and LL against ALA. Figure S3: Predictions about pharmacokinetic, toxicity and molecular targets, based on physicochemical properties for MTZ. Table S1: Paraclinical studies in hamsters with ALA and treated with KP and LL. Table S2: Bioinformatic analysis of potential pharmacophore targets of KP. Table S3: Bioinformatic analysis of potential pharmacophore targets of LL.

Author Contributions: Conceptualization, research, data collection and writing: preparation of the original draft, L.V.R. and J.A.V.D.; methodology, validation and formal analysis, V.I.H.R., H.V.R., E.B., M.H.M., R.D.C.M., B.C.M. and J.A.V.D.; writing: review editing, supervision, project administration and fund acquisition, F.C. and P.T.R. All authors have read and accepted the published version of the manuscript.

Funding: This research was funded by CONAHCYT and the Basic Science-Project (grant number: CB-2013-01-221136) to P.T.R.; J.A.V.D. (Reg. 103584) and H.V.R. (Reg. 371147) were recipients of postdoctoral fellowships by CONAHCYT.

Institutional Review Board Statement: This study was carried out in accordance with official Mexican regulations (NOM-062-ZOO-1999), and the protocol was approved by the Institutional Animal Care and Use Committee (Authorization No. 0183 -16) of the UPEAL-CINVESTAV-IPN.

Informed Consent Statement: Not applicable.

Data availability statement: All the data generated or analyzed during this study are included in this published article (as well as in the supplementary information files). The raw data are available from the corresponding author upon reasonable request.

Acknowledgments: The authors thank Jorge Fernández-Hernández, Benjamín Álvarez and Rafael Leiva (UPEAL-CINVESTAV) for the care and maintenance of the animals; Juan Carlos Osorio Trujillo and Daniel Morales-Mora for his technical help; Oliver Yemen Domínguez Flores and the ISSEMyM Imaging Diagnostic Service "Arturo Montiel Rojas" for the collaboration with the MRI studies; Anel Edith Lagunes-Guillén for her contribution with TEM studies; Carmen Selene Ramírez Vera (Merasoma Laboratory) for her help in the analysis of veterinary blood samples; and A. Palma (CMNS XXI Instrumentation Research Unit) for the support in obtaining the histological sections.

Conflicts of interest: The authors declare that they have no conflicts of interest. The funders had no role in the study design; in the collection, analysis or interpretation of data; in writing the manuscript; or in the decision to publish the results.

Abbreviations: ADME**:** absorption, distribution, metabolism and excretion; BBB, blood-brain barrier; BOILED, brain or intestinal estimated; CYP, cytochrome-P450 system; FLEX, flexibility; HBA, hydrogen bond acceptors; HBD, hydrogen bond donors; HIA, health impact assessment; INSATU, insaturation; INSOLU, insolubility; KP, kaempferol; LL, linearolactone; MCF, most common features; MTZ, metronidazole; NOX4, NADPH oxidase IV; OPRK, Kappa Opioid receptor; PGP, P-glycoprotein; pKa, acid dissociation coefficient; POLAR, polarity; PSA, polar surface area; LIPO, lipophilicity; Log P, partition coefficient; Log S, aqueous solubility coefficient; Vh, vehicle.

Appendix A

NC3R ARRIVE Guidelines Checklist.

 doi:10.20944/preprints202407.0797.v1

References

1. WHO (2017). Diarrheal disease. Available online: https://www.who.int/news-room/fact-sheets/detail/diarrhoeal-disease (accessed on 23 December 2020).
2. Shirley, D.A.; Hung, C.C.; Moonah, S. (2020). Part 5, Protozoal Infections: Chapter 94 - *Entamoeba histolytica* (Amebiasis). In *Hunter's Tropical Medicine and Emerging Infectious Diseases*, 10th ed.; Ryan, E.T., Hill, D.R., Solomon, T., Aronson, N.E., Endy, T.P., Eds.; Elsevier: Canada; pp. 699-706. ISBN: 978-0-323-55512-8. DOI: 10.1016/B978-0-323-55512-8.00094-6.
3. Gómez-García, C.; Marchat, L.A.; López-Cánovas, L.; Pérez-Ishiwara, D.G.; Rodríguez, M.A.; Orozco, E. (2017). Part - Parasitic Drug Resistance, Mechanisms: Chapter - Drug Resistance Mechanisms in *Entamoeba histolytica*, *Giardia lamblia*, *Trichomonas vaginalis*, and Opportunistic Anaerobic Protozoa. In *Antimicrobial Drug Resistance. Mechanisms of Drug Resistance*; 1st ed.; Mayers, D.L., Sobel, J.D., Oullette, M., Kaye, K.S., Marchaim, D., Eds.; Springer: Cham, Switzerland; pp. 613-628. ISBN 978-3-319-47264-5. DOI: 10.1007/978-3-319-46718-4_40.
4. Herrera-Martinez, M.; Hernández-Ramírez, V.I.; Hernández-Carlos, B.; Chávez–Munguía, B.; Calderón-Oropeza, M.A.; Talamás-Rohana, P. 2016. Antiamoebic activity of *Adenophyllum aurantium* (L.) Cystoskeleton of *Entamoeba histolytica*. Front Ethnopharmacol. Jun 27; 7:169.
5. VADEMECUM (2017). Metronidazole. Available online: https://www.vademecum.es/principios-activos-metronidazol-J01XD01 (accessed on 23 December 2020).
6. Tsai, J.P.; Hsieh, K.L.; Yeh, T.H.; Lee, Y.J.; Wei, C.R. (2019). The Occurrence of Metronidazole-Induced Encephalopathy in Cancer Patients: A Hospital-Based Retrospective Study. Annals of Indian Academy of Neurology, 22(3): 344-348. DOI: 10.4103/aian.AIAN_523_18.
7. Adil, M.; Iqbal, W.; Adnan, F.; Wazir, S.; Khan, I.; Khayam, M.U.; Kamal, M.A.; Ahmad, S.; Ahmed, J.; Khan, I.N. (2018). Association of Metronidazole with Cancer: A Potential Risk Factor or Inconsistent Deductions?. Current Drug Metabolism, 19(11): 902-909. DOI: 10.2174/1389200219666180329124130.
8. Quintanilla-Licea, R.; Vargas-Villarreal, J.; Verde-Star, M.J.; Rivas-Galindo, V.M.; Torres-Hernández, Á.D. (2020). Antiprotozoal Activity against *Entamoeba histolytica* of Flavonoids Isolated from *Lippia graveolens* Kunth. *Molecules*, 25(11): 2464. DOI: 10.3390/molecules25112464.
9. Llurba-Montesino, N.; Schmidt, T.J. (2018). *Salvia* Species as Sources of Natural Products with Antiprotozoal Activity. International Journal of Molecular Sciences, 19(1): 264. DOI: 10.3390/ijms19010264.
10. Calzada, F. (2005). Additional antiprotozoal constituents from *Cuphea pinetorum*, a plant used in Mayan traditional medicine to treat diarrhea. Phytotherapy Research, 19(8): 725-727. DOI: 10.1002/ptr.1717.
11. Bolaños, V.; Díaz-Martínez, A.; Soto, J.; Marchat, L.A.; Sánchez-Monroy, V.; Ramírez-Moreno, E. (2015). Kaempferol inhibits *Entamoeba histolytica* growth by altering cytoskeletal functions. Molecular and Biochemical Parasitology, 204(1): 16-25. DOI: 10.1016/j.molbiopara.2015.11.004.
12. Velázquez-Domínguez, J.A.; Hernández-Ramírez, V.I.; Calzada, F.; Varela-Rodríguez, L.; Pichardo-Hernández, D.L.; Bautista, E.; Herrera-Martínez, M.; Castellanos-Mijangos, R.D.; Matus-Meza, A.S.; Chávez-Munguía, B.; Talamás-Rohana, P. (2020). Linearolactone and kaempferol disrupt the actin cytoskeleton in *Entamoeba histolytica*: inhibition of amoebic liver abscess development. *Journal of Natural Products*, 83(12): 3671-3680. DOI: 10.1021/acs.jnatprod.0c00892.
13. Calzada, F.; Yepez-Mulia, L.; Tapia-Contreras, A.; Bautista, E.; Maldonado, E.; Ortega, A. (2010). Evaluation of the antiprotozoal activity of neo-clerodane type diterpenes from *Salvia polystachya* against *Entamoeba histolytica* and *Giardia lamblia*. Phytotherapy research, 24(5): 662-665. DOI: 10.1002/ptr.2938.
14. Diamond, L.S.; Harlow, D.R.; Cunnick, C.C. (1978). A new medium for the axenic cultivation of *Entamoeba histolytica* and other Entamoebas; Transactions of the Royal Society of Tropical Medicine and Hygiene, 72(4): 431-432. DOI: 10.1016/0035-9203(78)90144-x.
15. Argüello-García R, Calzada F, Chávez-Munguía B, Matus-Meza AS, Bautista E, Barbosa E, Velázquez, C., Hernández-Caballero ME, Ordoñez-Razo RM, Velázquez-Domínguez JA. Linearolactone Induces Necrotic-like Death in *Giardia intestinalis* trophozoites: Prediction of a Likely Target. (2022). Pharmaceuticals; 15(7):809. DOI: 10.3390/ph15070809.
16. Kalra, A.; Yetiskul, E.; Wehrle, C.J.; Tuma, F. (2020). Physiology, Liver. In *StatPearls* [Internet], 1st ed.; Abai, B., Abu-Ghosh, A., Acharya, A.B., *et al*., Eds.; StatPearls Publishing: Treasure Island, Florida, United State. Available online: https://www.ncbi.nlm.nih.gov/books/NBK535438/ (accessed on 23 December 2020).
17. Rovegno, M.; Vera, M.; Ruiz, A.; Benítez, C. (2019). Current concepts in acute liver failure. Annals of Hepatology, 18(4): 543-552. DOI: 10.1016/j.aohep.2019.04.008.

18. Lipinski, C.A.; Lombardo, F.; Dominy, B.W.; Feeney, P.J. (2001). Experimental and computational approaches to estimate solubility and permeability in drug discovery and development settings. Advanced drug delivery reviews, 46(1-3): 3-26. DOI: 10.1016/s0169-409x(00)00129-0.
19. Miao, J.; Chard, L.S.; Wang, Z.; Wang, Y. (2019). Syrian Hamster as an Animal Model for the Study on Infectious Diseases. Frontiers in immunology, 10(2329): 1-12. DOI: 10.3389/fimmu.2019.02329
20. Secretaría de Agricultura, Ganadería, Desarrollo Rural, Pesca y Alimentación (SAGARPA) (2001). Norma Oficial Mexicana NOM-062-ZOO-1999: Especificaciones técnicas para la producción, cuidado y uso de los animales de laboratorio. [Gobierno de México]. Disponible en: https://www.gob.mx/cms/uploads/attachment/file/203498/NOM-062-ZOO-1999_220801.pdf (Access: abril 20, 2023).
21. Percie du Sert, N.; Hurst, V.; Ahluwalia, A.; Alam, S.; Avey, M.T.; Baker, M.; Browne, W.J.; Clark, A.; Cuthill, I.C.; Dirnagl, U.; Emerson, M.; Garner, P.; Holgate, S.T.; Howells, D.W.; Karp, N.A.; Lazic, S.E.; Lidster, K.; MacCallum, C.J.; Macleod, M.; Pearl, E. J.; Würbel, H. (2020). The ARRIVE guidelines 2.0: Updated guidelines for reporting animal research. PLoS biology, 18(7): e3000410. DOI: 10.1371/journal.pbio.3000410
22. American Veterinary Medical Association (AVMA). (2020). AVMA Guidelines for the Euthanasia of Animals: 2nd Edition. Schaumburg, IL: AVMA.
23. Herrmann, K.; Flecknell, P. (2018). The application of humane endpoints and humane killing methods in animal research proposals: A retrospective review. Alternatives to laboratory animals: ATLA, 46(6)*:* 317-333. DOI: 10.1177/026119291804600606.
24. Organization for Economic Co-operation and Development (OECD). (2008). Section 4: Test no. 425, acute oral toxicity (up-and-down procedure). In: OECD Guidelines for the testing of chemicals, OECD (ed). OECD Publishing: Paris; 1-27. DOI: 10.1787/9789264071049-en.
25. Al Shoyaib, A.; Archie, S.R.; Karamyan, V.T. (2019). Intraperitoneal Route of Drug Administration: Should it Be Used in Experimental Animal Studies? Pharmaceutical research, 37(1): 12. DOI: 10.1007/s11095-019-2745-x
26. Secretaria de Salud (SSA) (2002). Norma Oficial Mexicana NOM-087-ECOL-SSA1-2002: Protección ambiental - Salud ambiental - Residuos peligrosos biológico-infecciosos -Clasificación y especificaciones de manejo [Gobierno de México]. Available from: http:// www.salud.gob.mx/unidades/cdi/nom/087ecolssa.html (Access: Abril 20, 2023).
27. Lindstrom, N.M.; Moore, D.M.; Zimmerman, K.; Smith, S.A. (2015). Hematologic assessment in pet rats, mice, hamsters, and gerbils: blood sample collection and blood cell identification. The veterinary clinics of North America. Exotic animal practice, 18(1): 21-32. DOI: 10.1016/j.cvex.2014.09.004
28. McKeon, G.P.; Nagamine, C.M.; Ruby, N.F.; Luong, R.H. (2011). Hematologic, serologic, and histologic profile of aged Siberian hamsters (*Phodopus sungorus*). Journal of the American Association for Laboratory Animal Science, 50(3): 308-316.
29. Foreman, J.H. (2023). Hyperlipemia and hepatic lipidosis in large animals. Available online: https://www.msdvetmanual.com/digestive-system/hepatic-disease-in-large-animals/hyperlipemia-and-hepatic-lipidosis-in-large-animals (accessed on 30 May 2023).
30. Flores, M.S.; Obregón-Cárdenas, A.; Tamez, E.; Rodríguez, E.; Arévalo, K.; Quintero, I.; Tijerina, R.; Bosques, F. & Galán, L. (2014). Hypocholesterolemia in patients with an amebic liver abscess. Gut and liver, 8(4): 415-420. DOI: 10.5009/gnl.2014.8.4.415
31. Fernández-Daza, E.; Fernández, J.E.; Moreno-Mejía, I.; Moreno-Mejía, M. (2008). Aproximación al diagnóstico de enfermedades hepáticas por el laboratorio clínico. Medicina & Laboratorio, 14(11-12*):* 533-546.
32. Zhang, J.; Wang, T.; Fang, Y.; Wang, M.; Liu, W.; Zhao, J.; Wang, B.; Wu, Z.; Lv, Y. & Wu, R. (2021) Clinical significance of serum albumin/globulin ratio in patients with pyogenic liver abscess. Frontiers in Surgery, 8: 677799. DOI: 10.3389/fsurg.2021.677799
33. Giannini, E.G.; Testa, R. & Savarino, V. (2005). Liver enzyme alteration: a guide for clinicians. *CMAJ:* Canadian Medical Association journal, 172(3): 367-379. DOI: 10.1503/cmaj.1040752
34. Lin, H.; Zhou, X. & Zhang, Z. (2022). The diagnostic value of GGT-based biochemical indicators for choledocholithiasis with negative imaging results of magnetic resonance cholangiopancreatography. Contrast media & molecular imaging, 2022(7737610): 1-10. DOI: 10.1155/2022/7737610.

 doi:10.20944/preprints202407.0797.v1

35. Tsutsumi, V.; Mena-López, R.; Anaya-Velázquez, F.; Martínez-Palomo, A. (1984). Cellular bases of experimental amebic liver abscess formation. The American journal of pathology, 117(1): 81-91.
36. Priyadarshi, R.N.; Kumar, R.; Anand, U. (2022). Amebic liver abscess: Clinico-radiological findings and interventional management. World Journal of Radiology, 14(*8*): 272-285. DOI: 10.4329/wjr.v14.i8.272.
37. Shibayama, M.; Campos-Rodríguez, R.; Ramírez-Rosales, A.; Flores-Romo, L.; Espinosa-Cantellano, M.; Martínez-Palomo, A.; Tsutsumi, V. (1998). *Entamoeba histolytica*: liver invasion and abscess production by intraperitoneal inoculation of trophozoites in hamsters, *Mesocricetus auratus*. Experimental parasitology, 88(1): 20-27. DOI: 10.1006/expr.1998.4218.
38. Denis, M.; Chadee, K. (1988). Immunopathology of *Entamoeba histolytica* infections. Parasitology today (Personal ed.), 4(9): 247-252. DOI: 10.1016/0169-4758(88)90139-1.
39. Krishna, M. (2014). Anatomía microscópica del hígado. Clinical liver disease, 2(Suppl 5): 109-112. DOI: 10.1002/cld.287.
40. Ghose, A.K.; Viswanadhan, V.N.; Wendoloski, J.J. (1999). A knowledge-based approach in designing combinatorial or medicinal chemistry libraries for drug discovery. 1. A qualitative and quantitative characterization of known drug databases. Journal of combinatorial chemistry, 1(1*):* 55-68. DOI: 10.1021/cc9800071.
41. Veber, D.F.; Johnson, S.R.; Cheng, H.Y.; Smith, B.R.; Ward, K.W.; Kopple, K.D. (2002). Molecular properties that influence the oral bioavailability of drug candidates. Journal of medicinal chemistry, 45(12): 2615-2623. DOI: 10.1021/jm020017n.
42. Egan, W.J.; Merz, K.M. Jr; Baldwin, J.J. (2000). Prediction of drug absorption using multivariate statistics. Journal of medicinal chemistry, 43(21): 3867-3877. DOI:10.1021/jm000292e.
43. Karthika, C.; Sureshkumar, R.; Zehravi, M.; Akter, R.; Ali, F.; Ramproshad, S.; Mondal, B.; Tagde, P.; Ahmed, Z.; Khan, F.S.; Rahman, M.H.; Cavalu, S. (2022). Multidrug resistance of cancer cells and the vital role of P-Glycoprotein. Life, 12(6): 897. DOI: 10.3390/life12060897.
44. Rajaram, R.D.; Dissard, R.; Jaquet, V.; De Seigneux, S. (2019). Potential benefits and harms of NADPH oxidase type 4 in the kidneys and cardiovascular system. Nephrology, dialysis, transplantation, 34(4): 567-576. DOI: 10.1093/ndt/gfy161.
45. Dalefield, M.L.; Scouller, B.; Bibi, R.; Kivell, B.M. (2022). The Kappa Opioid Receptor: A Promising Therapeutic Target for Multiple Pathologies. Frontiers in pharmacology, 13(837671*):* 1-26. DOI: 10.3389/fphar.2022.837671.
46. Brown, S.A. (2022). Renal dysfunction in small animals. Available online: https://www.msdvetmanual.com/urinary-system/noninfectious-diseases-of-the-urinary-system-in-small-animals/renal-dysfunction-in-small-animals (accessed on 30 May 2023).
47. Vicente, D. & Pérez-Trallero, E. (2010). Tetracyclines, sulfonamides, and metronidazole. Enfermedades infecciosas y microbiología clínica, 28(2): 122-130. DOI: 10.1016/j.eimc.2009.10.002.
48. Lala, V.; Zubair, M.; Minter, D.A. Liver Function Tests. [Updated 2022 Oct 5]. In: StatPearls [Internet]. Treasure Island (FL): StatPearls Publishing; 2023 Jan-. Available from: https://www.ncbi.nlm.nih.gov/books/NBK482489/.
49. Bansal, Y.; Maurya, V.; Tak, V.; Bohra, G.K.; Kumar, D.; Goel, A.D.; Yadav, T.; Nag, V.L. (2022). Clinical and laboratory profile of patients with amoebic liver abscess. Tropical parasitology, 12(2): 113-118. DOI: 10.4103/tp.TP_38_20.
50. Reyna-Sepúlveda, F.; Hernández-Guedea, M.; García-Hernández, S.; Sinsel-Ayala, J.; Muñoz-Espinoza, L.; Pérez-Rodríguez, E.; Muñoz-Maldonado, G. (2017). Epidemiology and prognostic factors of liver abscess complications in northeastern Mexico. Medicina Universitaria, 19(77): 178-183. DOI: 10.1016/j.rmu.2017.10.009
51. Hall, P. & Cash, J. (2012). What is the real function of the liver 'function' tests? The Ulster medical journal, 81(1): 30-36.
52. Loaeza-del-Castillo, A.; Paz-Pineda, F.; Oviedo-Cárdenas, E.; Sánchez-Ávila, F.; Vargas-Vorácková, F. (2008). AST to platelet ratio index (APRI) for the noninvasive evaluation of liver fibrosis. Annals of Hepatology, 7(4): 350-357. DOI: 10.1016/S1665-2681(19)31836-8
53. Feng, C.X.; Chen, X.Q.; He, X.L.; Lan, L.C.; Tang, Q.; Huang, L.; Shan, Q.W. (2022). Screening for Wilson's disease in acute liver failure: A new scoring system in children. Frontiers in pediatrics, 10: 1003887. DOI: 10.3389/fped.2022.1003887
54. Sueyoshi, S.; Sawai, S.; Satoh, M.; Seimiya, M.; Sogawa, K.; Fukumura, A.; Tsutsumi, M.; Nomura, F. (2016). Fractionation of gamma-glutamyltransferase in patients with nonalcoholic fatty liver disease and alcoholic liver disease. World journal of hepatology, 8(36): 1610-1616. DOI: 10.4254/wjh.v8.i36.161

55. Zhao, Z.; Zhu, Y.; Ni, X.; Lin, J.; Li, H.; Zheng, L.; Zhang, C.; Qi, X.; Huo, H.; Lou, X.; Fan, Q.; Bao, Y.; Luo, M. (2021). Serum GGT/ALT ratio predicts vascular invasion in HBV-related HCC. Cancer cell international, 21(1): 517. DOI: 10.1186/s12935-021-02214-1.
56. An, L.; Yin, W.T.; Sun, D.W. (2021). Albumin-to-alkaline phosphatase ratio as a promising indicator of prognosis in human cancers: is it possible? BMC cancer, 21(1): 247. DOI: 10.1186/s12885-021-07921-6.
57. Hulzebos, C.V.; Dijk, P.H. (2014). Bilirubin-albumin binding, bilirubin/albumin ratios, and free bilirubin levels: where do we stand? Seminars in perinatology, 38(7): 412-421. DOI: 10.1053/j.semperi.2014.08.004.
58. Choi, J.S.; Chung, K.S.; Lee, E.H.; Lee, S.H.; Lee, S.H.; Kim, S.Y.; Jung, J.Y.; Kang, Y.A.; Park, M.S.; Kim, Y.S.; Chang, J.; Leem, A.Y. (2020). The role of bilirubin to albumin ratio as a predictor for mortality in critically ill patients without existing liver or biliary tract disease. Acute and critical care, 35(1): 24-30. DOI: 10.4266/acc.2019.00738.
59. Pati, S.S.; Mishra, S.K.; Mohanty, S.; Pattnaik, J.K.; Das, B.S. (2003). Influence of renal impairment on plasma concentrations of conjugated bilirubin in cases of *Plasmodium falciparum* malaria. Annals of tropical medicine and parasitology, 97(6): 581-586. DOI: 10.1179/000349803225001418.
60. Rodríguez de Cossío, A.; Rodríguez-Sánchez, R. (2011). Pruebas de laboratorio en atención primaria (II). Medicina de Familia SEMERGEN, 37(3): 130-135. DOI: 10.1016/J.SEMERG.2010.12.003.
61. Brookes, E.M.; Power, D.A. (2022). Elevated serum urea-to-creatinine ratio is associated with adverse inpatient clinical outcomes in non-end stage chronic kidney disease. Scientific Reports, 12(20827): 1-10. DOI: 10.1038/s41598-022-25254-7.
62. Jorge Morales, B. (2010). Drogas Nefrotóxicas. Revista Médica Clínica Las Condes, 21(4): 623-628. DOI: 10.1016/S0716-8640(10)70578-2.
63. Ghosh, S.; Sharma, S.; Gadpayle, A.K.; Gupta, H.K.; Mahajan, R.K.; Sahoo, R.; Kumar, N. (2014). Clinical, laboratory, and management profile in patients of liver abscess from northern India. Journal of tropical medicine, 2014(142382): 1-8. DOI: 10.1155/2014/142382
64. Marie, C.S.; Verkerke, H.P.; Paul, S.N.; Mackey, A.J.; Petri, W.A. Jr. (2012). Leptin protects host cells from *Entamoeba histolytica* cytotoxicity by a STAT3-dependent mechanism. Infection and immunity, 80(5): 1934-1943. DOI: 10.1128/IAI.06140-11.
65. López-Contreras, L.; Hernández-Ramírez, V.I.; Herrera-Martínez, M.; Montaño, S.; Constantino-Jonapa, L.A.; Chávez-Munguía, B.; Talamás-Rohana, P. (2017). Structural and functional characterization of the divergent *Entamoeba* Src using Src inhibitor-1. Parasites & Vectors, 10(1): 500. DOI: 10.1186/s13071-017-2461-5.
66. Sladek, F.M. (2011). What are nuclear receptor ligands? Molecular and cellular endocrinology, 334(1-2): 3-13. DOI: 10.1016/j.mce.2010.06.018.
67. Bosch, D.E.; Siderovski, D.P. (2013). G protein signaling in the parasite *Entamoeba histolytica*. Experimental & molecular medicine, 45(3): e15. DOI: 10.1038/emm.2013.30.
68. Basith, S.; Cui, M.; Macalino, S.; Park, J.; Clavio, N.; Kang, S.; Choi, S. (2018). Exploring G protein-coupled receptors (GPCRs) ligand space via cheminformatics approaches: impact on rational drug design. Frontiers in pharmacology, 9(128): 1-26. DOI: 10.3389/fphar.2018.00128.
69. Valle-Solis, M.; Bolaños, J.; Orozco, E.; Huerta, M.; García-Rivera, G.; Salas-Casas, A.; Chávez-Munguía, B.; Rodríguez, M.A. (2018). A calcium/cation exchanger participates in the programmed cell death and *in vitro* virulence of *Entamoeba histolytica*. Frontiers in Cellular and Infection Microbiology, 8(342): 1-16. DOI: 10.3389/fcimb.2018.00342.
70. Li, S.; Yu, S.; Qin, J.; Peng, M.; Qian, J.; Zhou, P. (2022). Prognostic value of platelet count-related ratios on admission in patients with pyogenic liver abscess. BMC infectious diseases, 22(1): 636. DOI: 10.1186/s12879-022-07613-x.
71. Mosmann, T. (1983). Rapid colorimetric assay for cellular growth and survival: application to proliferation and cytotoxicity assays. Journal of immunological methods, 65(1-2): 55-63. DOI: 10.1016/0022-1759(83)90303-4
72. Varela-Rodríguez, L.; Sánchez-Ramírez, B.; Saenz-Pardo-Reyes, E.; Ordaz-Ortiz, J.J.; Castellanos-Mijangos, R.D.; Hernández-Ramírez, V.I.; Cerda-García-Rojas, C.M.; González-Horta, C.; Talamás-Rohana, P. (2021). Antineoplastic Activity of *Rhus trilobata* Nutt. (*Anacardiaceae*) against Ovarian Cancer and Identification of Active Metabolites in This Pathology. Plants, 10(10): 2074. DOI: 10.3390/plants10102074
73. Varela-Rodríguez, L.; Sánchez-Ramírez, B.; Rodríguez-Reyna, I.; Ordaz-Ortiz, J.J.; Chávez-Flores, D.; Salas-Muñoz, E.; Osorio-Trujillo, J.C.; Ramos-Martínez, E.; Talamás-Rohana, P. (2019). Biological and

toxicological evaluation of Rhus trilobata Nutt. (*Anacardiaceae*) used traditionally in Mexico against cancer. BMC Complement Altern Med 2019 Jul 1; 19(1):153.

74. Calzada F.; Meckes M.; and Cedillo-Rivera R.; 1999. Antiamebic and antigiardial activity of plant flavonoids; Planta Med. 65:78-80.
75. Chávez-Munguía, B.; Salazar-Villatoro, L.; Omaña-Molina, M.; Espinosa-Cantellano, M.; Ramírez-Flores, E.; Lorenzo-Morales, J.; Martínez-Palomo, A. (2016). Acanthamoeba culbertsoni: Electron-Dense Granules in a Highly Virulent Clinical Isolate. The Journal of eukaryotic microbiology, 63(6): 744-750. DOI: 10.1111/jeu.12321
76. Meneses-Ruiz, D.M.; Aguilar-Díaz, H.; Bobes, R.J.; Sampieri, A.; Vaca, L.; Laclette, J.P.; Carrero, J.C. (2015). Protection against Amoebic Liver Abscess in Hamster by Intramuscular Immunization with an Autographa californica Baculovirus Driving the Expression of the Gal-Lectin LC3 Fragment. BioMed research international, 2015(760598): 1-10. DOI: 10.1155/2015/760598
77. Herrera-Martínez, M.; Hernández-Ramírez, V.I.; Hernández-Carlos, B.; Chávez-Munguía, B.; Calderón-Oropeza, M.A.; Talamás-Rohana, P. (2016). Antiamoebic Activity of *Adenophyllum aurantium* (L.) Strother and Its Effect on the Actin Cytoskeleton of *Entamoeba histolytica*. Frontiers in pharmacology, 7(169): 1-13. DOI: 10.3389/fphar.2016.00169
78. Daina, A.; Michielin, O.; Zoete, V. (2017). SwissADME: a free web tool to evaluate pharmacokinetics, drug-likeness and medicinal chemistry friendliness of small molecules. Scientific reports, 7(42717): 1-13. DOI: 10.1038/srep42717
79. Daina, A.; Michielin, O.; Zoete, V. (2019). SwissTargetPrediction: updated data and new features for efficient prediction of protein targets of small molecules. Nucleic acids research, 47(1): 357-364. DOI: 10.1093/nar/gkz382
80. Sharma, A.K.; Srivastava, G.N.; Roy, A.; Sharma, V.K. (2017) ToxiM: A Toxicity Prediction Tool for Small Molecules Developed Using Machine Learning and Chemoinformatics Approaches. Frontier in Pharmacology, 8(880): 1-18. DOI: 10.3389/fphar.2017.00880.
81. Martin, T.; Harten, P.; Young, D. (2012). TEST (Toxicity Estimation Software Tool) Ver 4.1. U.S. Environmental Protection Agency, Washington, DC, EPA/600/C-12/006.
82. Banerjee, P.; Dunkel, M.; Kemmler, E.; Preissner, R. (2020). SuperCYPsPred-a web server for the prediction of cytochrome activity. *Nucleic acids research, 48(W1):* W580–W585. DOI: 10.1093/nar/gkaa166.
83. Maunz, A.; Gütlein, M.; Rautenberg, M.; Vorgrimmler, D.; Gebele, D.; Helma, C. (2013). lazar: a modular predictive toxicology framework. *Frontiers in pharmacology, 4(38):* 1-10. DOI: 10.3389/fphar.2013.00038.
84. Muegge, I.; Heald, S.L.; Brittelli, D. (2001). Simple selection criteria for drug-like chemical matter. Journal of medicinal chemistry, 44(12): 1841-1846. DOI: 10.1021/jm015507e.
85. Nigam, P.; Gupta, A.K.; Kapoor, K.K.; Sharan, G.R.; Goyal, B.M.; Joshi, L.D. (1985). Cholestasis in amoebic liver abscess. Gut, 26(2): 140-145. DOI: 10.1136/gut.26.2.140.
86. Chalasani, N.; Younossi, Z.; Lavine, J.E.; Charlton, M.; Cusi, K.; Rinella, M.; Harrison, S.A.; Brunt, E.M.; Sanyal, A.J. (2018). The diagnosis and management of nonalcoholic fatty liver disease: Practice guidance from the American Association for the Study of Liver Diseases. Hepatology (Baltimore, Md.), 67(1): 328-357. DOI: 10.1002/hep.29367.
87. Konigsfeld, H.P.; Viana, T.G.; Pereira, S.C.; Santos, T.O.C.D.; Kirsztajn, G.M.; Tavares, A.; De Souza Durão Junior, M. (2019). Acute kidney injury in hospitalized patients who underwent percutaneous kidney biopsy for histological diagnosis of their renal disease. BMC nephrology, 20(1): 315. DOI: 10.1186/s12882-019-1514-8.
88. Peng, K.Z.; Zhang, S.Y.; Zhou, H.L. (2016). Toxicological evaluation of the flavonoid-rich extract from Maydis stigma: Sub-chronic toxicity and genotoxicity studies in mice. Journal of ethnopharmacology, 192: 161-169. DOI: 10.1016/j.jep.2016.07.012.
89. Kebede, S.; Afework, M.; Debella, A.; Ergete, W.; Makonnen, E. (2016). Toxicological study of the butanol fractionated root extract of Asparagus africanus Lam., on some blood parameter and histopathology of liver and kidney in mice. BMC research notes, 9: 49. DOI: 10.1186/s13104-016-1861-5.
90. Agus, H.H. Chapter 4 - Terpene toxicity and oxidative stress. In Toxicology: Oxidative Stress and Dietary Antioxidants, 1st ed.; Patel, A.V.; Preedy, V.R. (Eds.); Academic Press: London, United Kingdom, 2021; Volume 1:33-42. DOI: 10.1016/B978-0-12-819092-0.00004-2.